Topological Zero-Modes and States of Self-Stress in 3D Lattices

THESIS

submitted in partial fulfillment of the
requirements for the degree of

MASTER OF SCIENCE
in
THEORETICAL PHYSICS

Author :	Guido Baardink
Student ID :	s1608444
Supervisor :	Vincenzo Vitelli
2^{nd} corrector :	Vadim Cheianov

Leiden, The Netherlands, February 24, 2017

Topological Zero-Modes and States of Self-Stress in 3D Lattices

Guido Baardink

Huygens-Kamerlingh Onnes Laboratory, Leiden University
P.O. Box 9500, 2300 RA Leiden, The Netherlands

February 24, 2017

Abstract

Mechanical metamaterials are structures whose carefully constructed geometry allows for unusual mechanical response. It has been shown that local rigidity and softness in isostatic structures may be described by a topologically protected polarization field. Here we exhaustively characterize a class of 3D lattices based on the 2D kagome lattice. Our main finding is a 3D metamaterial at critical mechanical stability, whose bottom side is much floppier than its top side. We also derive a general formula describing rigidity and softness associated to line dislocations in 3D polarized lattices.

Contents

Chapter 1

Introduction

Rigidity plays an essential role in architectural engineering (bridge building), but the mathematics of structural rigidity are also key in understanding mechanical properties of many materials, such as polymer networks and network glasses.

When modelled as ball-and-spring network, the rigidity and softness of these materials can be understood through comparing the degrees of freedom of the balls to the constraints imposed by the springs.

When not enough springs are present, the material can use the excess degrees of freedom for collective (infinitesimal) displacements that do not stretch or compress any of the springs (see Fig.1.1a). These zero-modes can be understood from the perspective of tunable softness [8] and could serve as mechanisms in molecular robotics.

On the other hand, if there is a surplus of springs, we can put a selection of them under tensions without producing any net forces on the balls (see Fig.1.1c). These pockets of self-stress could find applications in engineering the rigidity

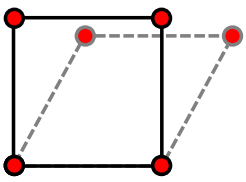

(a) *Soft frame. Zero-mode indicated by the gray dashed bonds.*

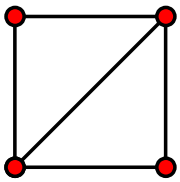

(b) *Marginally rigid frame. No mechanisms or states of self-stress.*

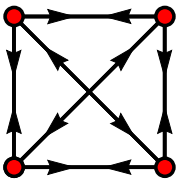

(c) *Rigid frame. State of self-stress indicated by the arrows.*

Figure 1.1: *A few examples of mechanical frames with $d \times N = 8$ and 2+1 rigid body movements, showing a transition from soft ($N_B < 8 - 3$) to rigid ($N_B > 8 - 3$) frames.*

Version of February 24, 2017– Created February 24, 2017 - 19:08

and fragility of materials.

In quantitative terms, given N balls connected in d dimensions by N_B springs, the Maxwell-Calladine index theorem [11, 12] reads

$$N_0 - N_S = d \times N - N_B, \tag{1.1}$$

where N_0 counts the independent bond-length-conserving displacements and N_S counts the independent ways to put the system under self-stress. Among these N_0 zero-modes, $d(d+1)/2$ are trivial rigid translations and rotations. The remaining zero-modes deform the structure internally and are known as mechanisms in engineering or floppy modes in physics. When both sides of this equation vanish we say that our system is isostatic or Maxwellian.

Recently, a theoretical link has been established between the fields of topological insulators and that of phononic crystals, strikingly exemplified by a mechanical analogue for the tight-binding model of graphene [9]. Fundamentally, this connection endows the latter field with the tools developed in quantum electronics [3]. Particularly in the case of Maxwell lattices, direct application of the basic topological methods will produce a topologically protected quantity that describes zero-modes and states of self-stress at a local level [2, 6, 7].

Much of the work up to this point has focused on the two-dimensional square and kagome lattices [1], the only three-dimensional implementation thus-far being on the pyrochlore lattice [5]. The drawback of this lattice is that its phonon spectrum contains Weyl lines, non-trivial structures of bulk zero-modes, which impede straightforward application of the topological methods.

Here, we show that a different three-dimensional lattice, constructed by stacking kagome lattices, can be deformed in such a way that its phonon spectrum is fully gapped. This property makes our lattice an ideal toy model in the study topological rigidity in three-dimensional materials.

In chapters 2 and 3, we derive the theoretical background from first principles. We introduce the Maxwell-Calladine index theorem within the context of rigidity theory and show how in isostatic lattices the localized version of the index takes on the form of a topologically protected polarization field.

Chapter 4 introduces the geometry under consideration, that is the generalized stacked kagome lattice. Next, chapter 5 describes how Weyl lines affect the polarization. Chapter 6 then shows that it is possible to completely gap the generalized stacked kagome lattice. Finally, in chapter 7 we derive a general formula describing rigidity and softness associated to line dislocations in three dimensional gapped isostatic lattices.

Version of February 24, 2017– Created February 24, 2017 - 19:08

Chapter 2

Rigidity theory

2.1 The Maxwell index

A lattice is a collection of sites (also called points, vertices) together with a collection of bonds (links, edges) between them. Assuming sites and bonds are neither destroyed nor created during our analysis, we label the sites and bonds enumeratively by $s \in \{1, \ldots, N\}$ and $\beta \in \{1, \ldots, N_B\}$. Each bond β signifies a link from a site s_β to a site s'_β and can be represented by the ordered pair $[s_\beta, s'_\beta]$. This completely captures the topology of our lattice.

We further add geometry by assigning equilibrium positions $\boldsymbol{R}(s) \in \mathbb{R}^d$ to all the sites. The bonds then obtain a geometric value of $\boldsymbol{b}_\beta = \boldsymbol{R}(s'_\beta) - \boldsymbol{R}(s_\beta)$, which we refer to as the separation vectors.

If we move the sites away from their initial positions, the length of the bonds between those sites might get stretched or compressed. If the displacements are sufficiently small compared to the lattice spacing, the relation between the displacement and elongations can be linearised.

Theorem 1. *If the displacements $\boldsymbol{u}$ are much smaller than the separations $\boldsymbol{b}_\beta$ then the elongation of the bonds is given by $e_\beta = \hat{\boldsymbol{b}}_\beta \cdot (\boldsymbol{u}(s'_\beta) - \boldsymbol{u}(s_\beta))$*

Proof. The elongation of a bond β is given explicitly by

$$\begin{aligned} e_\beta :&= ||\big(\boldsymbol{R}(s'_\beta) + \boldsymbol{u}(s'_\beta)\big) - \big(\boldsymbol{R}(s_\beta) + \boldsymbol{u}(s_\beta)\big)|| - ||\boldsymbol{R}(s'_\beta) - \boldsymbol{R}(s_\beta)|| \\ &= ||\boldsymbol{b}_\beta + \Delta_\beta \boldsymbol{u}|| - ||\boldsymbol{b}_\beta|| \qquad , \end{aligned} \tag{2.1}$$

where we have written $\Delta_\beta \boldsymbol{u} = \boldsymbol{u}(s'_\beta) - \boldsymbol{u}(s_\beta)$. Separation of $\Delta_\beta \boldsymbol{u}$ in parallel ($\Delta_\beta^{\parallel} \boldsymbol{u}$)

and orthogonal ($\Delta_\beta^\perp \boldsymbol{u}$) components with respect to $\hat{\boldsymbol{b}}_\beta$ gives

$$||\boldsymbol{b}_\beta + \Delta_\beta \boldsymbol{u}|| = \sqrt{||\boldsymbol{b}_\beta + \Delta_\beta^\parallel \boldsymbol{u}||^2 + ||\Delta_\beta^\perp \boldsymbol{u}||^2} \quad , \tag{2.2}$$

which can be expanded to obtain

$$||\boldsymbol{b}_\beta + \Delta_\beta \boldsymbol{u}|| = ||\boldsymbol{b}_\beta + \Delta_\beta^\parallel \boldsymbol{u}|| \left[1 + \mathcal{O}\left(\frac{||\Delta_\beta^\perp \boldsymbol{u}||^2}{||\boldsymbol{b}_\beta + \Delta_\beta^\parallel \boldsymbol{u}||^2}\right)\right]. \tag{2.3}$$

In the regime $||\boldsymbol{u}|| \ll ||\boldsymbol{b}||$ we can take the term in the square brackets to 1, to obtain

$$e_\beta = ||\boldsymbol{b}_\beta + \Delta_\beta^\parallel \boldsymbol{u}|| - ||\boldsymbol{b}_\beta|| = (b_\beta + \hat{\boldsymbol{b}}_\beta \cdot \Delta_\beta \boldsymbol{u}) - b_\beta = \hat{\boldsymbol{b}}_\beta \cdot (\boldsymbol{u}(s'_\beta) - \boldsymbol{u}(s_\beta)). \tag{2.4}$$

□

Similarly, varying the tension on the bonds might change the net forces on the sites. In the case of Hookean springs this is achieved by tuning the equilibrium length and/or spring constant of each spring. The relation between the forces $\boldsymbol{f}(s)$ and the tensions t_β is again linearised in the phonon limit. In fact, one can take $\boldsymbol{u}$ to zero to obtain

$$\boldsymbol{f}(s) = \sum_{\beta : s \in \beta} -\epsilon_{s,\beta} \hat{\boldsymbol{b}}_\beta t_\beta \quad \text{where} \quad \epsilon_{s,\beta} = \begin{cases} -1 & \text{if } s = s_\beta \\ +1 & \text{if } s = s'_\beta \end{cases} \quad , \tag{2.5}$$

where $\epsilon_{s,\beta}$ is defined such that $-\epsilon_{s,\beta}\hat{\boldsymbol{b}}_\beta$ always points *away* from s. If we extend $\epsilon_{s,\beta}$ to be zero whenever s is neither s_β nor s'_β, we can write Eq.(2.4) and Eq.(2.5) as

$$e_\beta = \sum_{s,i} \epsilon_{s,\beta} \hat{b}_{\beta,i}\, u_i(s) \quad \text{and} \quad f_i(s) = -\sum_\beta \epsilon_{s,\beta} \hat{b}_{\beta,i}\, t_\beta. \tag{2.6}$$

This can be expressed in matrix form by collecting all displacements resp. forces into dN-dimensional vectors and collecting all elongations resp. tensions into N_B-dimensional vectors, that is $U = (\boldsymbol{u}(1), \ldots, \boldsymbol{u}(N))$, $F = (\boldsymbol{f}(1), \ldots, \boldsymbol{f}(N))$, $E = (e_1, \ldots, e_{N_B})$ and $T = (t_1, \ldots, t_{N_B})$. Then Eq.(2.6) becomes

$$E = Q^T U \quad \text{and} \quad F = -QT, \tag{2.7}$$

where the elements of the $N_B \times dN$-dimensional rigidity matrix Q are given by $Q_{(s,i),\beta} = \epsilon_{s,\beta}\hat{b}_{\beta,i}$. The rigidity matrix Q is also called equilibrium matrix, and its transpose is often denoted C and called the compatibility matrix.

The rigidity matrix is an interesting object, as it gives us some insights on how the geometry affects the behaviour of the system, before any specific dynamics are introduced. In particular, the null-space of Q^T consists of non-zero displacements that do not elongate any bonds (up to first order in the displacement). If the only energy cost of deformations comes from stretching the bonds, these displacements can be excited spontaneously. As such we call them floppy modes, or zero-modes. It is important to remark that, since we are working in the linearised limit, we are dealing with infinitesimal displacements. The corresponding finite displacements might still stretch bonds.

Similarly the null-space of Q consists of non-zero bond tensions that do not give rise to any net forces on sites. This gives a configuration of the lattice where all sites are in equilibrium while some bonds are under tension. As such we call these states of self-stress. We denote the number of independent zero-modes by N_0 and the number of independent states of self-stress by N_S.

Because Q and Q^T are very intimately related, so are their kernels. In fact, using the rank-nullity theorem we have

$$\begin{aligned} \mathrm{rk}Q &= \dim \mathrm{dom}Q - \mathrm{null}Q = N_B - N_S \\ \mathrm{rk}Q^T &= \dim \mathrm{dom}Q^T - \mathrm{null}Q^T = dN - N_0 \end{aligned}, \tag{2.8}$$

which, by equality of column and row rank, reduces to the generalized Maxwell relation:

$$\nu = N_0 - N_S = dN - N_B. \tag{2.9}$$

This genuinely remarkable equality tells us that the difference between the number of zero-modes and the number of states of self-stress only depends on the number of sites and bonds in the lattice. All global deformations of the lattice that do not remove or add sites or bonds - changing the equilibrium positions or reconnecting bonds - keep ν invariant. As such, these deformations can only produce or destroy zero-modes and states of self-stress in pairs.

When ν is positive the lattice has more zero-modes than states of self-stress, implying a certain softness or malleability. On the other hand, negative ν implies a certain level of rigidity. When ν is zero each site has on average as many constraints as degrees of freedom, which we recognise as the isostatic condition. Lattices at this point of critical rigidity are also called Maxwellian.

2.2 Hamiltonian considerations

Let us consider the case where the bonds are Hookean springs with spring constant k and equilibrium length equalling the separation length $||\boldsymbol{b}_\beta||$. Then by

Hooke's law and Eq.(2.7) the potential energy contained in the lattice is

$$E_{\text{pot}} = \frac{k}{2} E^T E = \frac{k}{2} U^T Q Q^T U. \tag{2.10}$$

Which gives rise to the equation of motion

$$\ddot{U} = -\frac{k}{m} D U \quad with \quad D = Q Q^T, \tag{2.11}$$

where D is called the dynamic matrix. Clearly, calling the zero-eigenvectors of Q^T zero-energy modes, is only truly apt if they agree with the zero-eigenvectors of D. One inclusion, $\text{Ker}(Q^T) \subset \text{Ker}(D)$, is trivial from Eq.(2.11). Conversely, if $U \notin \text{Ker}(Q^T)$ then from

$$0 \neq \langle Q^T U | Q^T U \rangle = \langle U | Q Q^T U \rangle = \langle U | D U \rangle \tag{2.12}$$

we find $U \notin \text{Ker}(D)$. So indeed the kernels agree.

An interesting link to supersymmetry is discovered by expressing the equation of motion Eq.(2.11) in the form of a Schrödinger equation $i\frac{d}{dt}\psi = \mathcal{H}\psi$ through

$$\psi = \begin{pmatrix} i\dot{U} \\ Q^T U \end{pmatrix} \quad \text{and} \quad \mathcal{H} = \sqrt{\frac{k}{m}} \begin{pmatrix} 0 & Q \\ Q^T & 0 \end{pmatrix}. \tag{2.13}$$

In a certain sense this Hamiltonian is a Dirac inspired square root of the dynamical matrix, since

$$\mathcal{H}^2 = \begin{pmatrix} Q Q^T & 0 \\ 0 & Q^T Q \end{pmatrix} = \begin{pmatrix} D & 0 \\ 0 & \tilde{D} \end{pmatrix}. \tag{2.14}$$

Noting that $DQ = Q\tilde{D}$ and $\tilde{D}Q^T = Q^T D$ it is easy to see that $\tilde{D}$ has the same non-zero eigenvalues as D. Hence the non-zero eigenvalues of $\mathcal{H}$ are the square roots of the eigenvalues of D, all with doubled multiplicity.

On the other hand, the space of zero-eigenvectors of $\mathcal{H}$ is spanned by $(U, 0_{N_B})$ and $(0_{dN}, T)$, for U in the kernel of Q^T and T in the kernel of Q. Hence the nullity of $\mathcal{H}$ is the sum of the nullities of Q and Q^T.

In our supersymmetry analogy, the zero-energy modes are the super-partners of the states of self-stress, and can be distinguished by the parity operator $(-1)^F = \text{diag}(1_{dN}, -1_{N_B})$. Explicitly, zero-modes $(U, 0_{N_B})$ are simultaneous eigenvectors of $\mathcal{H}$ and $(-1)^F$ with the eigenvalues 0 and $+1$. Similarly, states of self-stress $(0_{dN}, T)$ are simultaneous eigenvectors with the eigenvalues 0 and -1.

Now we can use the tools of supersymmetry to re-express the Maxwell index theorem. Particularly we use the fact that for normal matrices A

$$\dim \ker A = \lim_{\epsilon \to 0} \epsilon \, \text{tr}(A + \epsilon I)^{-1}. \tag{2.15}$$

Version of February 24, 2017– Created February 24, 2017 - 19:08

For finite matrices this is easily seen by letting ϵ range over values larger than zero but smaller than the smallest positive eigenvalue of A (to ensure the invertibility of $A+\epsilon$). Then it is immediate that if A is normal, then so is $(A+\epsilon I)^{-1}$. Writing the trace as a sum over the eigenvalues λ_i of A we find

$$\lim_{\epsilon\to 0} \mathrm{tr}\frac{\epsilon}{A+\epsilon} = \sum_{i=1}^{n} \lim_{\epsilon\to 0} \frac{\epsilon}{\lambda_i+\epsilon} = \sum_{i=1}^{n} \delta_{0,\lambda_i} = \dim\ker A. \tag{2.16}$$

Applying this to the normal matrices D and $\tilde{D}$ we find

$$N_0 - N_S = \dim\ker D - \dim\ker\tilde{D} = \lim_{\epsilon\to 0}\left[\frac{\epsilon}{D+\epsilon} - \frac{\epsilon}{\tilde{D}+\epsilon}\right]. \tag{2.17}$$

Even more succinctly, since the zeroes of D and $\tilde{D}$ are zeroes of $\mathcal{H}$, distinguished by their eigenvalue from $(-1)^F$ we can write

$$\nu = N_0 - N_S = \lim_{\epsilon\to 0}\left[(-1)^F \frac{\epsilon}{\mathcal{H}+\epsilon}\right]. \tag{2.18}$$

While this equation is somewhat unwieldy for the global generalized Maxwell index, it provides a good starting point for localizing the Maxwell index, as considered in section 3.3.

2.3 Periodic lattices

Although the above theory applies in the more general case, it is often useful to consider the case of infinite periodic lattices.

Periodic lattices are constructed out of unit cells containing n sites at positions $\boldsymbol{R}_1,\ldots,\boldsymbol{R}_n$. These unit cells are then arranged periodically along primitive vectors $\boldsymbol{a}_i,\ldots,\boldsymbol{a}_d$, such that the complete set of lattice sites is given by

$$\boldsymbol{R}(s,\boldsymbol{\ell}) = \boldsymbol{R}_s + \sum_{i=1}^{d} \ell_i \boldsymbol{a}_i, \tag{2.19}$$

where $\boldsymbol{\ell}\in\mathbb{Z}^d$ is the lattice index, enumerating the different unit cells. The bonds can then be defined by n_B triples of the form

$$\beta = [s_\beta, s'_\beta, \Delta\boldsymbol{\ell}_\beta] \quad \text{such that} \quad \boldsymbol{b}_{\beta,\boldsymbol{\ell}} = \boldsymbol{R}(s'_\beta, \boldsymbol{\ell}+\Delta\boldsymbol{\ell}_\beta) - \boldsymbol{R}(s_\beta,\boldsymbol{\ell}). \tag{2.20}$$

Note that by the periodicity of the lattice we have $\boldsymbol{b}_{\beta,\boldsymbol{\ell}} = \boldsymbol{b}_{\beta,\boldsymbol{\ell}'}$ for any two lattice indexes $\boldsymbol{\ell}, \boldsymbol{\ell}'$. Hence we can drop the lattice index without loss of generality.

Version of February 24, 2017– Created February 24, 2017 - 19:08

The problem with considering infinite lattices is off course that our displacement and tension vectors become infinitely long as well. It is then natural to adopt a basis of plane waves satisfying

$$\boldsymbol{u}_{\boldsymbol{q}}(s,\,\boldsymbol{\ell}) = e^{\iota \boldsymbol{q}\cdot\sum_i \ell_i \boldsymbol{a}_i}\boldsymbol{u}_{\boldsymbol{q}}(s,\,\boldsymbol{0}), \tag{2.21}$$

where $U_q(\boldsymbol{\ell}) = (\boldsymbol{u}_{\boldsymbol{q}}(1,\,\boldsymbol{\ell}),\ldots,\boldsymbol{u}_{\boldsymbol{q}}(n,\,\boldsymbol{\ell}))$ is now a finite, but $\boldsymbol{q}$ dependent vector. We use $\iota = \sqrt{-1}$ for the imaginary unit, to allow i the role of index. For displacements of this form the bonds get elongated by

$$\begin{aligned} e_{\boldsymbol{q}}(\beta,\boldsymbol{\ell}) &= \hat{\boldsymbol{b}}_\beta \cdot \Big(\boldsymbol{u}_{\boldsymbol{q}}(s'_\beta,\,\boldsymbol{\ell}+\Delta\boldsymbol{\ell}_\beta) - \boldsymbol{u}_{\boldsymbol{q}}(s_\beta,\,\boldsymbol{\ell})\Big) = \hat{\boldsymbol{b}}_\beta \cdot \sum_s \epsilon_{s,\beta}\,\boldsymbol{u}_{\boldsymbol{q}}(s,\,\boldsymbol{\ell}+\delta_{s,s'_\beta}\Delta\boldsymbol{\ell}_\beta) \\ &= \sum_{s,i} \hat{b}_{\beta,i}\epsilon_{s,\beta}\,\exp\left[\iota\,\delta_{s,s'_\beta}\,\boldsymbol{q}\cdot\sum_j(\Delta\ell_\beta)_j\boldsymbol{a}_j\right] u_{\boldsymbol{q},i}(s,\,\boldsymbol{\ell}), \end{aligned} \tag{2.22}$$

where δ_{s,s'_β} is 1 if $s = s'_\beta$ and zero otherwise, and $\epsilon_{s,\beta}$ is ± 1 if s is either s'_β (+) or s_β (-) and zero otherwise. Collecting the bond elongations into the finite vector $E_q(\boldsymbol{\ell}) = (e_{\boldsymbol{q}}(1,\,\boldsymbol{\ell}),\ldots,e_{\boldsymbol{q}}(n_B,\,\boldsymbol{\ell}))$ we obtain the wave-number dependent relationship between the displacements and bond elongations

$$E_{\boldsymbol{q}}(\boldsymbol{\ell}) = C(\boldsymbol{q})U_{\boldsymbol{q}}(\boldsymbol{\ell}), \tag{2.23}$$

where we notice that the compatibility matrix is finite-dimensional and independent of the lattice index $\boldsymbol{\ell}$. Similarly we can collect the tensions in a n_B-dimensional vector $T_{\boldsymbol{q}}(\boldsymbol{\ell})$ and the forces in a dn-dimensional vector $F_{\boldsymbol{q}}(\boldsymbol{\ell})$ to obtain

$$-F_{\boldsymbol{q}}(\boldsymbol{\ell}) = Q(\boldsymbol{q})T_{\boldsymbol{q}}(\boldsymbol{\ell}), \tag{2.24}$$

with the Bloch representation of the rigidity matrix given by

$$Q_{(s,i),\beta}(\boldsymbol{q}) = \epsilon_{s,\beta}\hat{b}_{\beta,i}\exp\left[-\iota\,\delta_{s,s'_\beta}\,\boldsymbol{q}\cdot\textstyle\sum_{j=1}^{d}(\Delta\ell_\beta)_j\boldsymbol{a}_j\right] \tag{2.25}$$

and $C = Q^\dagger$. Again through the rank-nullity theorem we can find a wave-number dependent form of the Maxwell theorem

$$\nu(\boldsymbol{q}) = n_0(\boldsymbol{q}) - n_S(\boldsymbol{q}) = dn - n_B. \tag{2.26}$$

Finally we have to say a word about rigid transformations. For a finite lattice it is clear that moving all sites simultaneously in the same direction, or rotating all sites around a central point does not stretch any bonds. For periodic lattices the chosen boundary conditions prevent rigid rotations from being zero-energy,

as the choice of primitive vectors breaks rotational symmetry. However, rigid translations still remain free. That is, let $\boldsymbol{u_0}(s, \boldsymbol{\ell}) = \boldsymbol{v}$ for some $\boldsymbol{v} \in \mathrm{R}^d$, then

$$e_{\mathbf{0}}(\beta, \boldsymbol{\ell}) = \sum_{s,i} \hat{b}_{\beta,i}\, \epsilon_{s,\beta}\, e^0\, v_i = (\epsilon_{s_\beta,\beta} + \epsilon_{s'_\beta,\beta})\hat{\boldsymbol{b}}_\beta \cdot \boldsymbol{v} = 0. \tag{2.27}$$

So $U_{\mathbf{0}} = (\boldsymbol{v}, \boldsymbol{v}, \ldots, \boldsymbol{v})$ is a zero-eigenvector of $C(\mathbf{0})$ for any $\boldsymbol{v} \in \mathbb{R}^d$. As such we see that

$$n_0(\mathbf{0}) = \operatorname{null} C(\mathbf{0}) \geq d. \tag{2.28}$$

Version of February 24, 2017– Created February 24, 2017 - 19:08

Chapter 3

Topological mechanics

One of the most powerful ways to understand physical systems is through determining their invariants. In complex systems these conserved quantities give us some foothold to aid both our intuition as well as our calculations.

Most famously, one can find time-invariant quantities by studying continuous symmetries. Any continuous transformation of the system that leaves the Lagrangian invariant corresponds through Noether's theorem to a quantity g that satisfies $\frac{d}{dt}g = 0$. The connectedness of time then allows us to conclude that the quantity described by the function g will remain the same for all time to come (or - less poetically - until the symmetry breaks down).

In the study of quantum electronic systems it was realized that a different class of invariants can be found by considering the discrete symmetries of particle-hole duality and time-reversal symmetry. For a detailed description see [2, 3].

In its simplest form, topological mechanics is about finding conservation laws of the form

$$\underset{\text{connected}}{X} \xrightarrow{g} \underset{\text{discrete}}{Y} \quad : \quad g = \text{continuous} \iff g = \text{constant}. \tag{3.1}$$

While intuitively very clear, a somewhat needlessly strong proof that highlights the generality of the above statement is included in the appendix.

Within the framework of rigidity theory, we are working with time-reversal symmetric systems that respect the particle-hole symmetry $\{(-1)^F, \mathcal{H}\} = 0$. This places us in the symmetry class BDI, which suggests that we should look for winding numbers as candidates for the function g. Winding numbers are integers associated to functions that map a circle onto another circle. It expresses how many times the function wraps around the codomain each time it traverses the domain.

Version of February 24, 2017– Created February 24, 2017 - 19:08

Specifically we are looking for functions whose domain is a direct product of the circle S^1 with some other connected space X. Then, the winding number of this map will be a map from the connected space X to the discrete space $\mathbb{Z}$. That is, for functions $f : S^1 \times X \to S^1$ we obtain

$$g = \text{winding}[f] : X \to \mathbb{Z}. \tag{3.2}$$

The crucial realization is that Eq.(3.1) guarantees the winding number to be constant over X as long as g is continuous.

3.1 Winding numbers of the rigidity matrix

We recall the definition of the rigidity matrix in periodic lattices:

$$Q_{s,\beta}(\boldsymbol{k}) = \epsilon_{s,\beta}\hat{b}_{\beta,i} \exp\left[-\iota\, \delta_{s,s'_\beta} \boldsymbol{k} \cdot \Delta\boldsymbol{\ell}_\beta\right], \tag{3.3}$$

where we have chosen the orthonormal basis $k_i = \boldsymbol{q} \cdot \boldsymbol{a}_i$ for the Brillouin zone. Since the above expression remains invariant if $\boldsymbol{k}$ advances by 2π in any of the d basis directions, we can make the following identification

$$\boldsymbol{k} \in [0, 2\pi]^d \cong (S^1)^d = T^d, \tag{3.4}$$

i.e. the Brillouin zone is a d-torus. As such the rigidity matrix is a function of the form

$$Q : (S^1)^d \times X \to M_{dN \times N_B}(\mathbb{C}), \tag{3.5}$$

where X contains information on connectivity and geometry of the unit cells in the lattice, e.g. the values of the equilibrium positions $\boldsymbol{R}(s)$. Now suppose our lattice is Maxwellian, i.e. $dn = n_B$, then $Q(\boldsymbol{k})$ is a square matrix and we can take the determinant, returning a complex number. Further, wherever $\det Q \neq 0$ we can faithfully separate this number by magnitude and phase as $\det Q = |\det Q| e^{i\phi}$ such that

$$\phi : (S^1)^d \to S^1 : (k_1, \ldots, k_d) \mapsto \Im \ln \det Q(\boldsymbol{k}). \tag{3.6}$$

Since we have d circles we have d winding numbers:

$$m_i = \text{winding}_i \phi = \oint_{S^1_i} \frac{d\phi}{2\pi} = \int_0^{2\pi} \frac{dk_i}{2\pi} \frac{d}{dk_i} \Im \ln \det Q(\boldsymbol{k}). \tag{3.7}$$

Now to the issue of continuity. From Eq.(3.3) we see that the entries of the complex matrix valued function Q depend exponentially and thus continuously

on $\boldsymbol{k}$. Further we assume that Q depends continuously on the variables in X as well. By the continuity of the determinant $\det Q(\boldsymbol{k})$ is continuous as well.

The crucial step is the complex logarithm. Here, we notice that the phase of a complex continuous function can only change discontinuously if the function passes through zero. Hence, if we suppose the path in Eq.(3.7) does not cross the origin of the complex plane, we see that the winding numbers are the integral of a continuous function over a compact space. By the dominated convergence theorem, this means that the winding numbers are indeed continuous.

The take-home message is that, as long as we can guarantee that $\det Q \neq 0$ throughout the Brillouin zone, the winding numbers m_i are independent of $\boldsymbol{k}$ and any other variables contained in X. Lattices with this property are called gapped.

We have to mention the elephant in the room. From Eq.(2.28) we read that $\det Q(\boldsymbol{0}) = 0$ holds trivially, meaning that $\det Q \neq 0$ will never be realized throughout the entire Brillouin zone. Fortunately this problem can be circumnavigated by taking a closer look at the Brillouin zone. In two dimensions it is easy to see that any two S^1_i contours can be deformed into one-another without crossing the origin (Fig.3.1). The origin can therefore never be an obstruction to the constantness of the winding numbers.

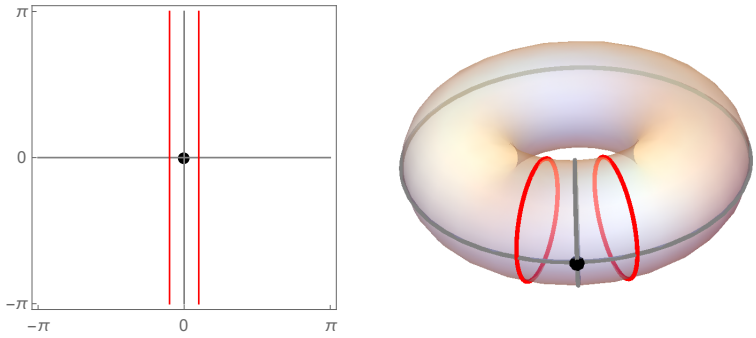

Figure 3.1: *Two contours (red lines) in a two-dimensional Brillouin zone on separate sides of the origin. On the left we have the standard visualization of the Brillouin zone where the left-right and top-bottom edges should be identified. On the right we have made this gluing explicit.*

In two dimensions a zero-mode away from the origin can form such an obstruction. However in higher dimensions we have enough freedom to move any contour around any isolated point, hence obstructions take the form of $d-2$ dimensional structures of zero-modes.

In summary, we have found we can assign topological invariants to gapped, periodic Maxwellian lattices. Now let us see what information is contained in these invariants.

Version of February 24, 2017– Created February 24, 2017 - 19:08

3.2 Zero-energy edge modes

The most straightforward interpretations of the winding numbers from the previous section is in terms of zero-energy edge modes. For this, we consider wave numbers with non-zero imaginary component, that is $k_i \mapsto k_i + \iota\kappa_i$. Comparing with Eq.(2.21) we see that this corresponds to exponentially decaying waves

$$\boldsymbol{u}_{\boldsymbol{k}+\iota\boldsymbol{\kappa}}(s,\boldsymbol{\ell}) = e^{-\boldsymbol{\ell}\cdot\boldsymbol{\kappa}}\, e^{\iota\boldsymbol{\ell}\cdot\boldsymbol{k}}\, \boldsymbol{u}_{\boldsymbol{k}+\iota\boldsymbol{\kappa}}(s,\boldsymbol{0}). \tag{3.8}$$

Clearly on infinite lattices these waves inevitably grow to a point where the displacement $\boldsymbol{u}$ fails to be small with respect to the lattice spacing. However, on finite lattices the situation is quite different.

Consider the edge of a finite lattice, for simplicity let the edge be perpendicular to the j-th primitive vector such that $\boldsymbol{a}_j$ points outwards. Then, the displacement vectors with negative κ_j will be confined to this edge. Recalling that the index $(s,\boldsymbol{\ell})$ corresponds to the position $\boldsymbol{R}_s(\boldsymbol{\ell}) = \boldsymbol{R}_s + \sum_i \ell_i \boldsymbol{a}_i$, we can write

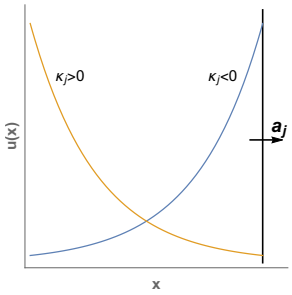

Figure 3.2: *Decay direction dependence on κ_j.*

$$|\boldsymbol{u}_{\boldsymbol{k}+\iota\kappa_j\boldsymbol{e}_j}(\boldsymbol{x})| \propto e^{-\kappa_j(\boldsymbol{x}\cdot\boldsymbol{a}_j)}. \tag{3.9}$$

If $\kappa_j < 0$, the growth is in the direction of $\boldsymbol{a}_j$, that is towards the edge. If $\kappa_j > 0$, the growth is opposite the direction of $\boldsymbol{a}_j$ (see Fig.3.2). Canonically orienting ourselves such that $\boldsymbol{a}_j$ points to the right, we say that if κ_j is positive (negative) it is confined to the left (right) edge with penetration depth $|\kappa_j|^{-1}$. When $\kappa_j = 0$ the penetration depth becomes infinite, the mode neither grows nor decays and now constitutes a lattice-spanning bulk mode.

Since the rigidity matrix only depends on the wave numbers through complex exponentials $e^{\iota k_i}$ and $e^{-\iota k_i}$, we consider the variables $z_i = e^{\iota(k_i+\iota\kappa_i)}$. This allows us to write

$$\det Q(\boldsymbol{k}+\iota\boldsymbol{\kappa}) = \mathcal{Q}(z_1,\ldots,z_k), \tag{3.10}$$

for some rational function $\mathcal{Q}: \mathbb{C}^d \to \mathbb{C}$. Considering a system with only those edges that are perpendicular to the j-th primitive vector, we must have $|z_i| = 1$ for all $i \neq j$. Then $|z_j| < 1$ corresponds to a right edge mode, $|z_j| > 1$ to a left edge mode and $|z_j| = 1$ to a bulk mode, as shown in Fig.3.3. Now, we can consider the meromorphic function

$$\mathcal{Q}_j : \mathbb{C} \to \mathbb{C} : z_j \mapsto \mathcal{Q}(e^{\iota k_1},\ldots,e^{\iota k_{j-1}}, z_j, e^{\iota k_{j+1}},\ldots,e^{\iota k_d}), \tag{3.11}$$

which depends implicitly on all $(k_i)_{i\neq j}$. Recalling the definition of the winding numbers from Eq.(3.7), we know how to rewrite the winding numbers in terms

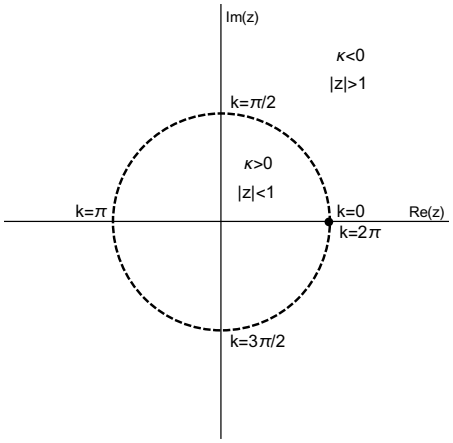

Figure 3.3: *The embedding of one dimension of the Brillouin zone (dashed line) in the complex plane. The dot indicates the origin of the Brillouin zone.*

of a contour integral in the complex plane

$$m_j = \oint_{S^1_j} \frac{d\phi}{2\pi} = \oint_{|z_j|=1} \frac{d \ln \mathcal{Q}_j}{2\pi\imath} = n_j^{right} - p_j^{right}, \tag{3.12}$$

where, to find the second equality, the real part of $\oint d \ln \mathcal{Q}$ can be ignored, as $\ln|\det Q|$ is a continuous real-valued function. The last equality follows from the Cauchy argument principle, which states that this particular contour integral evaluates to the number of zeroes n_j^{right} of $\mathcal{Q}_j$ enclosed by the contour (counted with multiplicity), minus the number of enclosed poles p_j^{right} of $\mathcal{Q}_j$ (counted with order). The superscript expresses the fact that points enclosed by the contour satisfy $|z| < 1$ and thus correspond to modes confined to the right edge.

This equation is an example of the boundary-bulk correspondence prevalent in many applications of topological theories. In our case the winding numbers, defined in terms of bulk-modes, give us information about the existence of zero-energy modes confined to edges. The equation Eq.(3.12) is very reminiscent of the Maxwell relation Eq.(2.9), with a topologically restricted constant on the left and a difference involving zero modes on the right hand side. In fact, we will see in the next section that there is a very strong correspondence between the winding numbers and a localized version of the Maxwell index.

As a final note we remark that, since $\mathcal{Q}_j$ depends implicitly on the variables k_i for $i \neq j$, one would naively expect this dependence to be transferred to n_j^{right} and p_j^{right}. However if the lattice is fully gapped we know that the left hand side of Eq.(3.12) is topologically constant. This fixes the difference $n_j^{right} - p_j^{right}$ to a

constant as well. It is interesting to consider what happens if the lattice is not fully gapped. We will return to this question in Chapter 5.

3.3 Local rigidity in isostatic lattices

Interestingly and surprisingly the winding numbers also show up when localizing the Maxwell relation Eq.(2.9). To motivate this localization from a theoretical perspective, it is useful to think of zero-modes and states of self-stress as mechanical analogues of electric charges. In this light the generalized Maxwell relation is a global rigidity charge conservation law: no matter how much the lattice is deformed the number of zero-modes can only change if the number of states of self-stress changes by the same amount.

Continuing this analogy, it would be interesting to have an analogue for the Gauss law in electromagnetism. That is, a rigidity polarization density function $\boldsymbol{P}_T$ such that for any region S in a periodic, gapped Maxwellian lattice the total rigidity charge contained in the region S can be obtained through

$$\nu^S = \oint_{\partial S} \boldsymbol{P}_T \cdot d^{d-1}\boldsymbol{S}. \tag{3.13}$$

We follow the argument by Kane and Lubensky and define the quantity on the left hand side as

$$\nu^S = N_0^S - N_{SS}^S := \text{null}\Big[\rho_S(\mathbf{r})Q^\dagger\Big] - \text{null}\Big[\rho_S(\mathbf{r})Q\Big], \tag{3.14}$$

where r is the diagonal matrix containing the positions of the sites and the average positions of the bonds on its diagonal, and $\rho_S : \mathbb{R}^d \to \mathbb{R}$ is a smoothed indicator function, evaluating to 1 on the interior of S, quickly dropping to zero over the edge of S and remaining zero outside S. With Eq.(2.15) we have

$$\nu^S = \lim_{\epsilon\to 0} \text{tr}\left[(-1)^F \rho_S(\mathbf{r}) \frac{\iota\epsilon}{\mathcal{H} + \iota\epsilon}\right]. \tag{3.15}$$

We first extract the part that corresponds with the nullity in the rank-nullity theorem, counting the bond-deficiency

$$\nu_L^S = \lim_{\epsilon\to 0} \text{tr}\left[(-1)^F \rho_S(\mathbf{r})\right] \propto dN^S - N_B^S, \tag{3.16}$$

where the subscript L indicates that this quantity concerns local counts. The remainder $\nu_T^S = \nu^S - \nu_L^S$, called the topological count, can be expressed as

$$\nu_T^S = \lim_{\epsilon\to 0} \text{tr}\left[(-1)^F \rho_S(\mathbf{r}) \frac{-\mathcal{H}}{\mathcal{H} + \iota\epsilon}\right] = \lim_{\epsilon\to 0} \frac{1}{2}\text{tr}\left[(-1)^F \frac{1}{\mathcal{H} + \iota\epsilon}[\rho_S(\mathbf{r}), \mathcal{H}]\right]$$

Version of February 24, 2017– Created February 24, 2017 - 19:08

through the anti-commutation relation $\{(-1)^F, \mathcal{H}\} = 0$ and the cyclic property of the trace. We note that the commutator evaluates to zero wherever ρ_S is constant, hence only the boundary of S contributes. We approximate $[\rho_S(\mathbf{r}), \mathcal{H}] \equiv [\mathbf{r}, \mathcal{H}] \cdot \nabla\rho_S(\mathbf{r})$ and assume that $\mathcal{H}$ is gapped along the boundary ∂S to safely let ϵ go to zero, and obtain

$$\nu_T^S = \frac{1}{2}\mathrm{tr}\left[\nabla\rho(\mathbf{r}) \cdot (-1)^F \mathcal{H}^{-1}[\mathbf{r}, \mathcal{H}]\right]. \tag{3.17}$$

Next suppose the boundary region is periodic, so we can use the plane wave basis detailed in Eq.(2.21) to evaluate the trace. In this basis the position operator can be re-expressed as $\mathrm{r} \sim \imath\nabla_{\boldsymbol{q}}$. For any wave number, evaluating the commutator in this basis amounts to

$$\begin{aligned}(-1)^F \mathcal{H}^{-1}[\nabla_{\boldsymbol{q}}, \mathcal{H}] &= \begin{pmatrix} 1 & 0 \\ 0 & -1 \end{pmatrix} \begin{pmatrix} 0 & Q^{\dagger -1} \\ Q^{-1} & 0 \end{pmatrix} \begin{pmatrix} 0 & \nabla_{\boldsymbol{q}} Q \\ \nabla_{\boldsymbol{q}} Q^\dagger & 0 \end{pmatrix} \\ &= \begin{pmatrix} Q^{\dagger -1}\nabla_{\boldsymbol{q}} Q^\dagger & 0 \\ 0 & -Q^{-1}\nabla_{\boldsymbol{q}} Q \end{pmatrix},\end{aligned} \tag{3.18}$$

where we used $[\partial, V]f = (\partial V)f$ for any potential V acting on any vector f. Taking the trace of the above we obtain

$$\frac{\iota}{2}\left(\mathrm{tr}[Q^{-1}\nabla_{\boldsymbol{k}} Q]^* - \mathrm{tr}[Q^{-1}\nabla_{\boldsymbol{k}} Q]\right) = \mathrm{Im}\,\mathrm{tr}[Q^{-1}\nabla_{\boldsymbol{k}} Q]. \tag{3.19}$$

Using the corollary from Jacobi's formula $\mathrm{tr}\log = \log\det$ and the linearity of the imaginary part and the trace we find

$$\mathrm{Im}\,\mathrm{tr}\, Q^{-1}\nabla_{\boldsymbol{q}} Q = \mathrm{Im}\,\mathrm{tr}\nabla_{\boldsymbol{q}} \log Q = \nabla_{\boldsymbol{q}} \mathrm{Im}\log\det Q = \nabla_{\boldsymbol{q}}\phi(\boldsymbol{q}). \tag{3.20}$$

Noting that the divergence points to the direction of steepest ascent, we see that $\nabla\rho(\mathrm{r})$ evaluates to the *inwards* normal $\hat{\boldsymbol{n}}$ of the boundary ∂S.

$$\nu_T^S = \int_{\partial S} d^{d-1}S\, \hat{\boldsymbol{n}} \cdot \int_{BZ} \frac{d^d\boldsymbol{q}}{(2\pi)^d} \nabla_{\boldsymbol{q}}\phi(\boldsymbol{q}). \tag{3.21}$$

Comparing with Eq.(3.7) and Eq.(3.13) we see that our polarization charge obtains the form

$$\boldsymbol{P}_T = \sum_i m_i \boldsymbol{a}_i, \tag{3.22}$$

where m_i are the winding numbers from Eq.(3.7).

Version of February 24, 2017– Created February 24, 2017 - 19:08

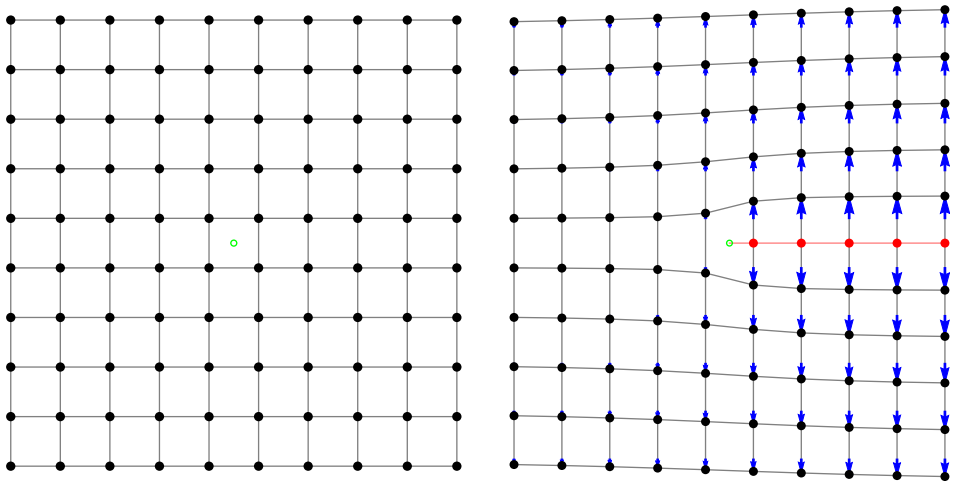

Figure 3.4: *Point dislocation in a 2D lattice. Depicted on the left is a generic 2D square lattice where black points represent centres of unit cells. On the right the blue arrows show the displacement field and the extra row of unit cells in red. The green circle indicates the dislocation center.*

3.4 Dislocations in periodic lattices

In order to apply the theory from the previous section, we are looking for a region of a lattice whose boundary is in a locally gapped, periodic Maxwellian lattice. The trivial example is any region in a globally gapped, periodic Maxwellian lattice. However, a fully periodic lattice is homogeneous and hence has constant polarization and thus zero net flux through any closed boundary. This should not be surprising, since by definition Maxwellian lattices have $\nu = 0$, and by homogeneity it is easy to argue that this descends to the local level $\nu_T^S = 0$.

Hence we need to modify our lattice set-up such that the polarization is non-constant. That is, we would like to have either the winding number or the primitive vectors vary. The former can be accomplished by gluing two lattices with different polarization together, creating domain walls as shown in [2].

The latter, more subtle way of creating regions of non-constant polarization can be accomplished by introducing dislocations to the lattice. We want to make a local distortion of the lattice in such a way that far away from that distortion the lattice looks perfectly periodical and undisturbed. We do this by introducing a displacement function $\boldsymbol{u}(\boldsymbol{x})$ that acts on the lattice by displacing sites at position $\boldsymbol{x}$ to the position $U(\boldsymbol{x}) = \boldsymbol{x} + \boldsymbol{u}(\boldsymbol{x})$. The dislocation itself is a singularity of the function $\boldsymbol{u}(\boldsymbol{x})$: a region L where the derivatives of $\boldsymbol{u}(\boldsymbol{x})$ are ill-defined, that is to say a region where $\boldsymbol{u}$ is markedly not smooth. A typical example of a

dislocation in a two-dimensional lattice is shown in Fig.3.4.

If we want our lattice to be periodical far away from the dislocation, we must have that far away from L the function $\boldsymbol{u}(\boldsymbol{x})$ is nearly constant *modulo primitive vectors*. For if the displacement jumps by a primitive vector $\boldsymbol{a}_i$ we can still connect the unit cell to the next unit cell over in the i-th direction. At these points of discontinuity we require the derivatives of $\boldsymbol{u}$ to exist and agree in the limit on both sides of the discontinuity, to ensure smoothness far from the dislocation.

Then, for any loop C around the defect we must have that the total change of $\boldsymbol{u}$ around that loop is an integer multiple of primitive vectors

$$\boldsymbol{b} := \int_C d\boldsymbol{u} \in \sum_i \mathbb{Z}\boldsymbol{a}_i. \tag{3.23}$$

This quantity, called the Burgers vector [10], depends continuously on the chosen path and maps to a discrete set. As such we recognise it as a topological invariant satisfying Eq.(3.1). In fact let A be a surface such that the loop C corresponds to the boundary ∂A, then

$$\boldsymbol{b} = \int_{\partial A} d\boldsymbol{u} = \int_A d(d\boldsymbol{u}) = \int_A \sum_{i<j} \left[\partial_i, \partial_j\right] \boldsymbol{u}\, dx^i \wedge dx^j. \tag{3.24}$$

Since the derivatives of the displacement function are smooth away from the dislocation, we conclude that the only part of the integral that contribute is the region $A \cap L$.

If the dimension of the dislocation is exactly two lower than the dimension of the lattice, or more exactly if $\mathbb{R}^d \setminus L$ is homotopic to the circle, we can conscientiously express the integral of $d\boldsymbol{u}$ over any path C as a winding number

$$\int_C d\boldsymbol{u} = \boldsymbol{b}\,\mathrm{Winding}(C, L), \tag{3.25}$$

clearly showing its topological properties.

3.5 Rigidity charge associated to dislocations

Far away from the dislocation the lattice looks undisturbed. As the polarization vector is a local quantity, we must have that in these regions it differs only infinitesimally from the dislocation-free case. Remember that the expression for the polarization is

$$\boldsymbol{P}(\boldsymbol{x}) = \sum_i m_i(\boldsymbol{x})\boldsymbol{a}_i(\boldsymbol{x}). \tag{3.26}$$

Since the winding numbers m_i are integers they cannot carry the infinitesimal change. Hence we turn our attention to the primitive vectors.

The primitive vector field $\boldsymbol{a}_i(\boldsymbol{x})$ is a constant vector field such that if $\boldsymbol{x}$ is a position in the unit cell $\boldsymbol{a}_i(\boldsymbol{x})$ is the same position in the next unit cell in the i-th direction. Under a dislocation displacement both unit cells get deformed, hence the origin and the destination of this vector need to be considered:

$$\begin{aligned}\tilde{\boldsymbol{a}}_i(\boldsymbol{x}) &= U(\boldsymbol{x}+\boldsymbol{a}_i) - U(\boldsymbol{x}) \\ &= \boldsymbol{a}_i + \boldsymbol{u}(\boldsymbol{x}+\boldsymbol{a}_i) - \boldsymbol{u}(\boldsymbol{x}) \\ &\approx \boldsymbol{a}_i + (\boldsymbol{a}_i\cdot\nabla)\boldsymbol{u}(\boldsymbol{x}),\end{aligned} \tag{3.27}$$

where the last step assumes that the higher derivatives are negligible.

The volume of a unit cell can be expressed as the volume of the parallelotope constructed from the primitive vectors $\boldsymbol{a}_i$. Explicitly if we have the matrix $A_{ij} = \boldsymbol{a}_i\cdot\hat{\boldsymbol{e}}_j$, where $\{\hat{\boldsymbol{e}}_i\}_{1\le i\le d}$ forms an orthogonal basis, then the volume is

$$V_{cell} = |\det A|\,. \tag{3.28}$$

As we know how the primitive vectors behave under the distortion we can proceed to calculate the distorted volume

$$\begin{aligned}\tilde{V}_{cell} &= \det[\tilde{\boldsymbol{a}}_1,\dots,\tilde{\boldsymbol{a}}_d] = \det[\boldsymbol{a}_1+(\boldsymbol{a}_1\cdot\nabla)\boldsymbol{u},\dots,\boldsymbol{a}_d+(\boldsymbol{a}_d\cdot\nabla)\boldsymbol{u}] \\ &= \det[\boldsymbol{a}_1,\dots,\boldsymbol{a}_d] + \sum_i \det[\boldsymbol{a}_1,\dots,(\boldsymbol{a}_i\cdot\nabla)\boldsymbol{u},\dots,\boldsymbol{a}_d] + \mathcal{O}^2(\partial u).\end{aligned} \tag{3.29}$$

The summation can be simplified by expansion in cofactors C_{ij}

$$\begin{aligned}\sum_i \det[\boldsymbol{a}_1,\dots,(\boldsymbol{a}_i\cdot\nabla)\boldsymbol{u},\dots,\boldsymbol{a}_d] &= \sum_i\sum_j\sum_k a_{ik}\partial_k u_j C_{ij} \\ &= \sum_j\sum_k \partial_k u_j \sum_i a_{ik}C_{ij} = \sum_j\sum_k \partial_k u_j(\delta_{jk}\det A),\end{aligned} \tag{3.30}$$

To linear order in ∂u we find

$$\tilde{V}_{cell}(\boldsymbol{x}) = V_{cell}(1+\nabla\cdot\boldsymbol{u}(\boldsymbol{x})). \tag{3.31}$$

Thus, if the boundary of S is taken far away from the dislocation deep inside a region where the lattice is gapped, periodic and Maxwellian, we find with the above expansions to first order in the displacements

$$\nu_T^S = \int_{\partial S}\frac{d^{d-1}S}{\tilde{V}_{cell}}\tilde{\boldsymbol{P}}\cdot\hat{\boldsymbol{n}} = \int_{\partial S}\frac{d^{d-1}S}{V_{cell}}\hat{n}_i\left[P_i + P_j\partial_j u_i - P_i\partial_j u_j\right]. \tag{3.32}$$

Using the divergence theorem this reduces to

$$\nu_T^S = \int_S \frac{dV}{V_{cell}} - \partial_i \left[P_i + P_j \partial_j u_i - P_i \partial_j u_j \right] = - \int_S \frac{dV}{V_{cell}} P_i \left[\partial_i, \partial_j \right] u_j. \tag{3.33}$$

From this equation the relation to the Burgers vector Eq.(3.24) is clear. We see that, in a sense, the rigidity charge is a direct consequence of a failure of partial derivatives to commute at the dislocation singularity. Naturally, from a mathematical standpoint this analysis is somewhat problematic, as the derivatives are ill-defined at the singularity. We shall return to a mathematically more rigorous argument in Chapter 7.

Chapter 4

The stacked kagome lattice

The theory of topological mechanics has been mostly developed on the one-dimensional polyacetalene chain and the two-dimensional kagome lattice. The latter case, owing its name to a weaving pattern used in traditional Japanese basketry, is built up out of triangular unit cells arranged in such a way that the sides of the triangles form straight lines across the lattice, as shown in Fig.4.1.

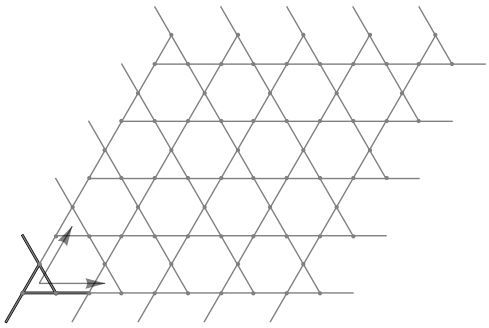

Figure 4.1: *The 2D kagome lattice, with one unit cell highlighted and primitive vectors $\boldsymbol{a}_1$ and $\boldsymbol{a}_2$ drawn.*

When the triangles are twisted and deformed, while keeping the primitive vectors and connectivity the same, we obtain a fully gapped lattice. Our aim is to construct a three-dimensional gapped lattice, using this two-dimensional lattice as a building block.

Perhaps the most straightforward extension of the kagome model to three dimensions is by layering these two-dimensional sheets and connecting those sheets vertically. This is accomplished by adding a third primitive vector perpendicular to the other two:

$$\boldsymbol{a}_1 = a(1,0,0) \quad \boldsymbol{a}_2 = a(1/2,\sqrt{3}/2,0) \quad \boldsymbol{a}_3 = a(0,0,1) \ , \tag{4.1}$$

Version of February 24, 2017– Created February 24, 2017 - 19:08

where a defines the lattice spacing.

This addition of a third lattice vector readily generates the desired stacking of the triangular unit cells. However, to allow for a broader range of control over the deformations of the unit cell, we extend our unit cell to contain a vertical pair of triangles. That is, the equilibrium positions of the sites in the unit cell form the following triangular prism:

$$\begin{array}{lll} \boldsymbol{R}(1) = -\frac{1}{4}\boldsymbol{a}_3 & \boldsymbol{R}(2) = \frac{1}{2}\boldsymbol{a}_1 - \frac{1}{4}\boldsymbol{a}_3 & \boldsymbol{R}(3) = \frac{1}{2}\boldsymbol{a}_2 - \frac{1}{4}\boldsymbol{a}_3 \\ \boldsymbol{R}(4) = +\frac{1}{4}\boldsymbol{a}_3 & \boldsymbol{R}(5) = \frac{1}{2}\boldsymbol{a}_1 + \frac{1}{4}\boldsymbol{a}_3 & \boldsymbol{R}(6) = \frac{1}{2}\boldsymbol{a}_2 + \frac{1}{4}\boldsymbol{a}_3 \end{array} . \tag{4.2}$$

We shall refer to the sites $s = 1, 2, 3$ as the bottom triangle and to the sites $s = 4, 5, 6$ as the top triangle of the unit cell. The eighteen bonds are then induced by connecting each site to its six nearest neighbours, as shown in Fig.4.2.

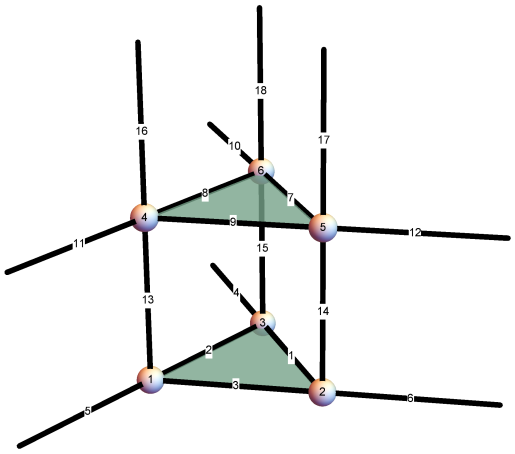

Figure 4.2: *The unit cell of the stacked kagome lattice, with sites and bonds numbered.*

After numbering the bonds we can write down the rigidity for this matrix rather explicitly, which we have done in the appendix. Independent on the numbering, the determinant of the rigidity matrix of the above lattice is

$$\det Q(z_1, z_2, z_3) = \frac{3^3}{2^6}(z_1 z_2)^{-2}(1 - z_1)^2(1 - z_2)^2(1 - z_3)^3(z_1 - z_2)^2, \tag{4.3}$$

where $z_i(\boldsymbol{q}) = e^{\imath k_i(\boldsymbol{q})} = e^{-\imath \boldsymbol{q}\cdot\boldsymbol{a}_i}$. Thus we find the determinant of the rigidity matrix to be zero along the four planes in momentum space given by $k_i = 0$ and $k_1 = k_2$. Our goal is to remove these zero-structures.

Version of February 24, 2017– Created February 24, 2017 - 19:08

4.1 Unit cell deformations

We look to deform the triangular prism unit cell by varying the equilibrium positions of all six sites, hoping to find a configuration with the property that $\det Q(\boldsymbol{k})$ is non-zero for all non-zero $\boldsymbol{k}$. Each site has three degrees of freedom for a total of 18 degrees. Although our lattice provides several symmetries that we could use to remove some trivial degrees of freedom, we would still be left with a rather large-dimensional problem. Instead we choose to restrict our problem to deformations that are easily conceptualized. The guiding principle is to play with the orientation of the top and bottom triangle, while keeping their shape equilateral and their side lengths exactly one half of the lattice spacing

This leaves us with nine degrees of freedom, three for the orientation of each triangle and three for the relative position of their centres. For the orientation of the triangle we consider the following dynamic orthogonal frame. Imagine first taking the line through the center of the triangle perpendicular to the triangle surface. Second we draw the angle bisector line of any angle of the triangle. Finally we define the line through the center of the triangle that is perpendicular to both those lines. Note that, no matter how we orient the triangle, these lines defined in this way stay perpendicular.

Any orientation can be reached by rotating the triangle around these three dynamical axes according to a triple of angles (ψ, ϕ, θ). First we can rotate the triangle around the vertical axis by an angle ψ. Then we can roll the triangle

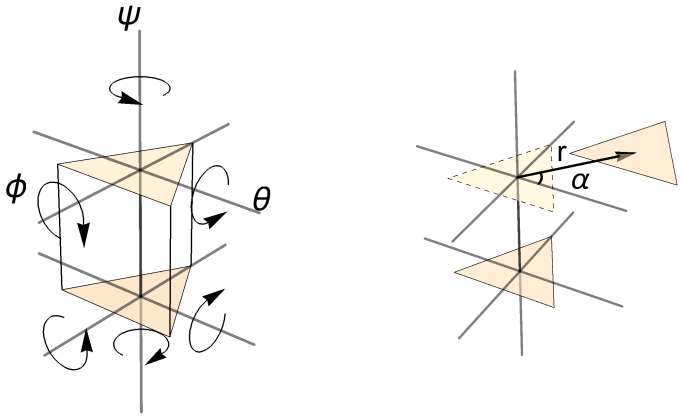

(a) *Rotation deformations.* ***(b)*** *Translation deformations.*

Figure 4.3: *The two types of unit cell deformations.*

over the axis given by the angle bisector under an angle ϕ. Finally we tilt the triangle by an angle θ around the axis that is now perpendicular to both the central axis and the angle bisector. One advantage of keeping the axes of rotation dynamic, apart from easing the intuition, is that our rotations commute with one another.

To further restrict our phase space, we invert the orientation of the top and bottom triangle, e.g. if the top triangle is turned clockwise, then the bottom triangle turns anticlockwise. For example, a non-zero angle ψ will twist the prism as if to wring out a we towel. Finally we keep the vertical distance between the planes constant. In the end we are left with five parameters, three for the orientation of the triangles, and two for the relative *horizontal* separation of the triangles. The action of each of these parameters on the stacked kagome unit cell is illustrated in Fig.4.3

4.2 One-parameter deformations

To get a feel for the effect of the deformation parameters on the zeroes of the rigidity matrix we discuss the determinant of each of the deformations separately. Firstly, we note that the determinant of the rigidity matrix is invariant under the sheering induced by a non-zero r. That is to say, for non-zero r we retain:

$$\det Q_r(z_1, z_2, z_3) = -\frac{3^3}{2^6}(z_1 z_2)^{-1}(1-z_1)^2(1-z_2)^2(1-z_3)^3(z_1-z_2)^2. \quad (4.4)$$

We easily see that this expression vanishes only for $z_i = 1$ or $z_1 = z_2$. In terms of wave-numbers these solutions correspond for the four planes $k_1 = 0$, $k_2 = 0$, $k_3 = 0$ and $k_1 = k_2$ in the Brillouin zone.

However, any reorientation of the triangles causes us to lose some zero-structures. Non-zero θ or ϕ cause us to lose the planes $k_2 = 0$ and $k_1 = k_2$. A caveat is that the specific angles $(\psi, \phi, \theta) \in \{(0, 0, \frac{\pi}{3}), (0, 0, \frac{\pi}{2}), (0, \frac{\pi}{2}, 0)\}$ cause the lattice to become singular, meaning that $\det Q = 0$ everywhere.

The situation gets a bit more interesting when we get to the rotations around the vertical axis. In this case the $k_1 = 0$ plane breaks down to the single line $k_1 = k_2 = 0$. Thus, for non-zero ψ the only zero-mode structures are the $k_3 = 0$ plane and the k_3-axis.

The analytic calculations for finding the above structures is deferred to the appendix. All zero-energy bulk-modes can be succinctly visualized in Fig.4.4 and listed in Table 4.1. Sadly but unsurprisingly we see that a one-parameter deformation is not sufficient to completely gap the lattice. Hence we turn our attention to composite deformations.

Version of February 24, 2017– Created February 24, 2017 - 19:08

Table 4.1: *Zero-mode structures for the four one-parameter deformations.*

Non-zero par.	*Planes*	*Lines*
none	$k_3 = 0, k_1 = 0, k_2 = 0, k_1 = k_2$	
(r, α)	$k_3 = 0, k_1 = 0, k_2 = 0, k_1 = k_2$	
θ	$k_3 = 0, k_1 = 0$	
ϕ	$k_3 = 0, k_1 = 0$	
ψ	$k_3 = 0$	$k_1 = k_2 = 0$

Figure 4.4: *Locus of zero modes for different one-parameter deformations of the unit cell. On the left we have the spectrum of a lattice without any re-orientation of the triangles, in the middle of the lattice at non-zero ϕ or θ rotations and on the right of the lattice at non-zero ψ.*

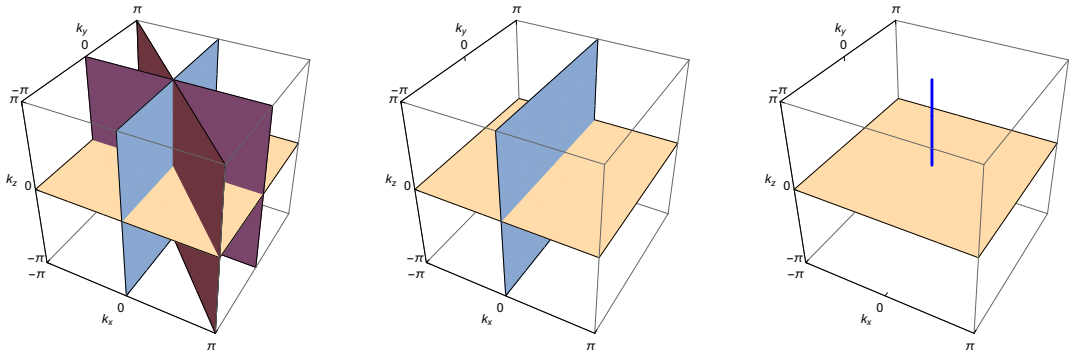

4.3 Composite deformations on the k_3 axis

We found two zero-mode structures that were invariant under one-parameter deformations: the $k_3 = 0$ plane and the k_3 axis. If we restrict our attention to the k_3 axis, we can give complete analytical expressions for the combined action of up to three variables. First we observe what a general re-orientation of the triangles does to the k_3 axis. Given any value of the three angles ψ, ϕ and θ the corresponding determinant is

$$\begin{aligned}\det Q_{\psi\theta\phi}(1,1,z_3) = -\frac{3^4}{2}(1-z_3)^3(1-\cos\theta\cos\phi)^2\cos^2\theta\cos^2\phi\sin^4\psi \\ \cdot\Big[2\cos\theta(3\cos\theta+4\cos\phi)-\cos 2\phi(\cos 2\theta-3) \\ -4\cos 2\psi(1+\cos\theta\cos\phi)^2\Big]. \quad (4.5)\end{aligned}$$

We observe that the k_3 axis is either completely zero or completely gapped.

Version of February 24, 2017– Created February 24, 2017 - 19:08

Next, in the case of non-zero r we set each the angles to zero in turn. It turns out that all these combinations are also proportional to $(1-z_3)^3$, which allows us to write

	$\det Q_{r\psi\phi\theta}(1,1,z_3)/(1-z_3)^3$
$\psi=0$	0
$\phi=0$	$2^2 3^4 \sin^4\theta \sin^4\psi (r^2\cos^2\alpha \sin^2\theta - \cos^2\theta \sin^2\psi)$
$\theta=0$	$2^2 3^4 \sin^4\phi \sin^4\psi (r^2\sin^2\alpha \sin^2\phi - \cos^2\phi \sin^2\psi)$

From the first row of the table we conclude that a non-zero ψ is a necessary condition to gap the k_3-axis, while r seems to play a minor role at best. In fact, we observe that the combination of actions $\psi, \phi \in (0, -\pi/2)$ or $\psi, \theta \in (0, -\pi/2)$ does the trick. Hence we will focus our attention on exploring these phase spaces. At this point it stops being feasible to approach the problem analytically and we will start relying on numerical computations.

Chapter 5

Weyl lines

5.1 Weyl loops

We remember from section 3.1 that the winding numbers as defined in Eq.(3.7) are invariants if the determinant of the rigidity matrix is non-zero everywhere in the Brillouin zone apart from the origin. Let us consider what happens if this condition is not satisfied. For simplicity we will first restrict ourselves to the two-dimensional case. Suppose our rigidity matrix has a zero at the point $(\tilde{k}_1, \tilde{k}_2)$, with both wave numbers for the sake of argument non-zero. The difference between two winding numbers calculated around circles on either side of the zero is

$$m_2(k_1^>) - m_2(k_1^<) = \int_{S_2^1(k_1^>)} d\phi - \int_{S_2^1(k_1^<)} d\phi = \int_C d\phi, \tag{5.1}$$

where C is a small loop around the zero point, see Fig.5.1.

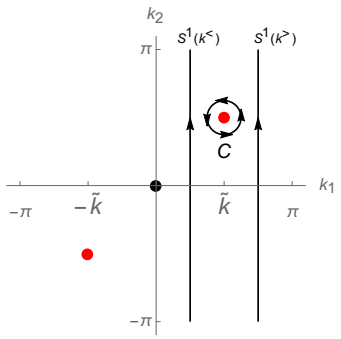

Figure 5.1: *Two S^1 contours on different sides of a zero point in the interior of the Brillouin zone.*

We observe that if the right hand side vanishes, then the winding numbers around each circle are equal, and we obtain that m_2 is still invariant. For this reason, zeroes for which $\int_C d\phi$ is zero are called topologically trivial. The non-trivial zeroes then are called the Weyl points of the lattice.

Note in particular that the integral in Eq.(5.1) is mostly independent of the particular loop C. The only requirement being that the loop must be the (exterior) boundary of a surface that contains the zero point. However, note that in higher dimensions the choice of surface fails to be unique. As such we must conclude that *an isolated zero in a three-dimensional Brillouin zone is always trivial.* In fact it is not hard to imagine that the lowest-dimensional non-trivial zero-structures must be closed lines. These lines are what we call Weyl lines.

Not all lines of zero-modes are Weyl lines. For instance in the lattice corresponding to $(\psi, \phi, \theta) = (\frac{\pi}{3}, 0, 0)$ we have shown the k_3 axis to be a line of zero modes (cf. Fig.4.4), however it is clear that all horizontal lines can be deformed into each other without crossing the central axis. This can be made somewhat more explicit by rewriting Eq.(A.13) to

$$\det Q_{\psi=\frac{\pi}{3}}(k_1, k_2, k_3) = \frac{3^4}{2^4}(1 - e^{\imath k_3})^3 \left[\cos k_1 + \cos k_2 + \cos(k_1 - k_2) - 3\right]^2 . \quad (5.2)$$

Then taking any loop C with constant k_3 around the k_3 axis will return

$$\int_C d\phi_{\psi=\frac{\pi}{3}} = 3 \int_C d \circ \arg(1 - e^{\imath k_3}) = 0 \quad (i = 1, 2), \quad (5.3)$$

showing that this line is topologically trivial indeed.

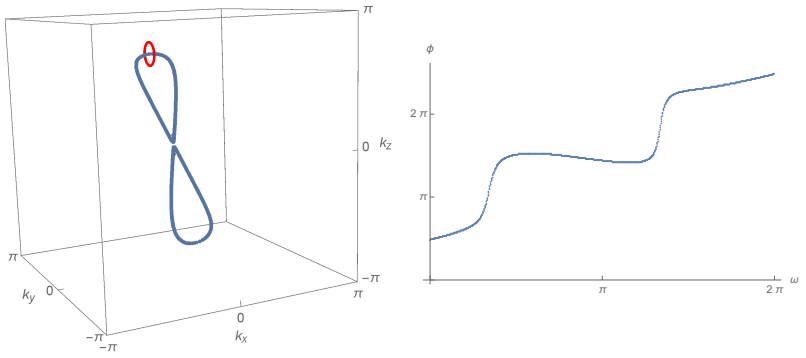

(a) ***(b)***

Figure 5.2: *a) Sampling of the Weyl loop at $(\psi, \phi, \theta) = (\frac{\pi}{4}, \frac{5\pi}{12}, 0)$. Closer to the origin the sampling becomes less reliable. b) Phase of the rigidity matrix around the red circular contour in a) parametrized by the angle ω.*

By a similar argument the horizontal plane is not an obstruction to moving horizontal S^1_i-contours around and is in that sense trivial. We conclude that for the $(\psi, \phi, \theta) = (\frac{\pi}{3}, 0, 0)$ the horizontal winding numbers (m_1, m_2) are invariant wherever they are defined.

Weyl lines in three dimensional Maxwellian lattices have already been described in the case of the generalized pyrochlore lattice [5], consisting of lines from the origin of the Brillouin zone to the origin of a Brillouin zone one reciprocal lattice vector ahead. That is, these Weyl lines completely traverse a direction of the 3-torus. What is novel in the stacked kagome lattice, is the existence of closed loops that do not traverse the Brillouin zone, showing greater potential for shrinking them to the origin. We call these structures Weyl loops.

The most extensive Weyl loop found in our analysis is depicted in Fig.5.2, together with a visual proof of topological non-triviality. On the other end of the size spectrum we seem to find a series of parametrizations that produce arbitrarily small Weyl loops, as depicted in Fig.5.3. In the next chapter we will find that this shrinking can completely eliminate the Weyl loop.

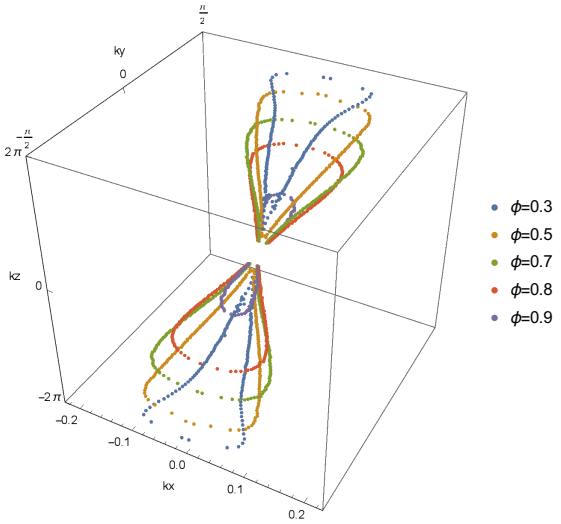

Figure 5.3: *Sampling of the Weyl structures at $\psi = \pi/3$ and $\theta = 0$ for different values of ϕ. As ϕ grows towards $1 \approx \pi/3$ we see the Weyl loop shrink into the origin.*

5.2 Edge signature

From Eq.(5.1) we read that in lattices with Weyl lines the winding numbers are no longer constant. In fact by consulting Fig.5.2b we see that by crossing the Weyl line the winding numbers will change by unity. As we know that the

Version of February 24, 2017– Created February 24, 2017 - 19:08

winding numbers encode the number of zero-modes on the right edge, we expect a zero mode to flip from one to the other edge when crossing the Weyl line.

This relation between the zero-energy edge modes and the zero-energy bulk modes is arguably best demonstrated by Fig.5.4, showing the complex plane from Fig.3.3 with an extra degree of freedom. At different values of k_1 we might find the corresponding zero mode either at the top ($|z_3(k_1)| < 1$) or bottom ($|z_3(k_1)| > 1$) edge, or in the bulk ($|z_3(k_1)| = 1$). However, by continuity of these zero-energy structures we know that if a mode changes side, it must pass through a non-trivial bulk zero.

Intuitively this can be understood by realizing that, as $|z_3|$ approaches 1 the penetration depth diverges, allowing it to hop between sides. A particularly aesthetically pleasing example of this side switching is shown in Fig.5.5.

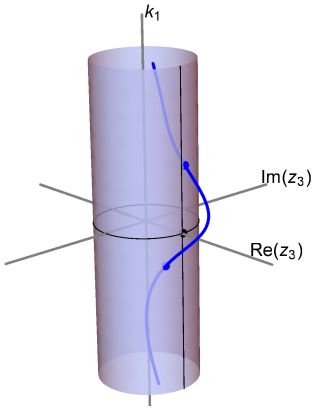

Figure 5.4: *A zero mode changing edge. The Brillouin zone is indicated by the cylindrical hull, with the axis and origin of the Brillouin zone indicated by the thin black lines.*

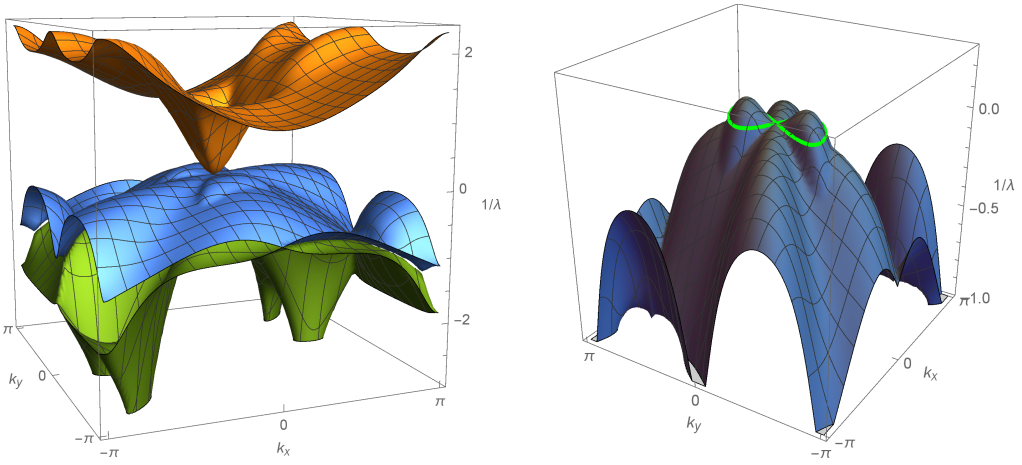

(a) ***(b)***

Figure 5.5: *Zero-energy edge modes bound to horizontal edges for the lattice corresponding to $(\psi, \phi, \theta) = (\frac{\pi}{4}, \frac{5\pi}{12}, 0)$. In a) all three bands are shown, while in b) the middle band isolated with the Weyl loop drawn in green at $\lambda = \infty$. The vertical axis indicates the inverse penetration depth $1/\lambda = \ln|z_i|$ where negative (positive) λ indicates modes bound to the right (left) edge.*

Version of February 24, 2017– Created February 24, 2017 - 19:08

Chapter 6

Gapping the kagome lattice

6.1 Soft directions

One thing all the observed Weyl lines have in common is the fact that they form a connected path to the origin of the Brillouin zone. This suggests the following conjecture

Conjecture 1. *All Weyl Lines are connected to the origin.*

This allows us to turn our attention to infinitesimal spheres around the origin. If our function is gapped there the conjecture guarantees that the function is gapped in the entire Brillouin zone. The advantage is that, instead of the polynomials of trigonometric functions involved in finding Weyl lines, the problem of finding these soft directions (see Fig.6.1) is a statement about shared real zeroes of low degree homogeneous polynomials. The latter is computationally much more feasible, allowing us to sweep the complete phase space of triangle orientations, with sufficient resolution to distinguish the important features, overnight.

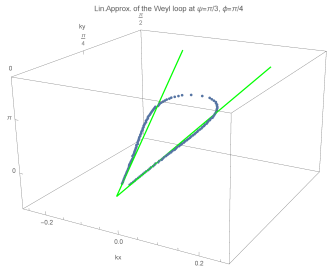

Figure 6.1: *The linear approximation (green) to the Weyl line sampling (blue) at* $(\psi, \phi, \theta) = (\frac{\pi}{3}, \frac{\pi}{4}, 0)$*, indicating the soft directions. Only half of the Brillouin zone is shown.*

To investigate the neighbourhood of the origin, we expand the determinant of the rigidity matrix around $\boldsymbol{k} = 0$. Recalling that the rigidity matrix depends on $\boldsymbol{k}$ only through the complex exponentials $e^{\pm \imath k_i}$ we can write down a general form for the expansion

$$\det Q(\boldsymbol{k}) = \sum_{\boldsymbol{n}} c_{\boldsymbol{n}} e^{-\imath \boldsymbol{n}\cdot\boldsymbol{k}} = \sum_{\boldsymbol{n}} \sum_{m} \frac{(-\imath)^m}{m!} c_{\boldsymbol{n}} (\boldsymbol{n}\cdot\boldsymbol{k})^m = \sum_{m} \frac{(-\imath)^m}{m!} P_m(\boldsymbol{k}), \qquad (6.1)$$

where $P_m(\boldsymbol{k}) = c_{\boldsymbol{n}}(\boldsymbol{n}\cdot\boldsymbol{k})^m$ are homogeneous polynomials of degree m with real coefficients in three real variables k_1, k_2 and k_3. The first three polynomials (the constant, linear and quadratic terms) vanish identically. This is a reflection of the dimension of the kernel of $Q(\mathbf{0})$ being at least $d = 3$ (cf. Eq.(2.28)) and is proven in the appendix.

Since the polynomials are entirely real, we read from Eq.(6.1) that the real (complex) part of $\det Q(\boldsymbol{k})$ is given by summation over the even (odd) degree polynomials. If $\det Q(\boldsymbol{k})$ is to be zero somewhere on the infinitesimally small sphere around the origin, then both the lowest order real and the lowest order complex polynomial have to vanish there. That is, we must have a common real zero of the third and forth polynomial. This is made rigorous in the following lemma.

Lemma 1. *If the rigidity matrix Q is zero along a path γ that connects to the origin, then the corresponding third and fourth homogeneous polynomials satisfy*

$$P_3(\hat{\boldsymbol{k}}) = P_4(\hat{\boldsymbol{k}}) = 0 \quad \textit{where} \quad \hat{\boldsymbol{k}} = \left.\frac{d\gamma}{d||\gamma||}\right|_{||\gamma||=0}.$$

Proof. As our path connects to the origin we can choose a parametrization such that $\gamma(0) = \mathbf{0}$. Since this is a minimum of $||\gamma||$ we can find a small interval $[0,\delta)$ on which $||\gamma||$ is strictly increasing. On this interval we can re-parametrize γ by its length:

$$\gamma : [0, ||\gamma(\delta)||) \to \mathbb{R}^3 : \epsilon \mapsto \epsilon\hat{\gamma}_\epsilon \quad \text{s.t.} \quad ||\hat{\gamma}_\epsilon|| = 1. \tag{6.2}$$

Then we can use the homogeneity of the polynomials to find

$$\begin{aligned} 0 &= \Im \det Q(\gamma(\epsilon)) = \textstyle\sum_{m\geq 1} \frac{(-1)^{m+1}}{(2m+1)!}\epsilon^{2m+1} P_{2m+1}(\hat{\gamma}_\epsilon) \\ 0 &= \Re \det Q(\gamma(\epsilon)) = \textstyle\sum_{m\geq 2} \frac{(-1)^{m}}{(2m)!}\epsilon^{2m} P_{2m}(\hat{\gamma}_\epsilon) \end{aligned}. \tag{6.3}$$

We can find a very rough upper bound for the homogeneous polynomials over the unit sphere by

$$|P_m(\hat{\gamma}_\epsilon)| = \left|\sum_{\boldsymbol{n}} c_{\boldsymbol{n}}(\boldsymbol{n}\cdot\hat{\gamma}_\epsilon)^m\right| \leq \sum_{\boldsymbol{n}} |c_{\boldsymbol{n}}|\,|\boldsymbol{n}\cdot\hat{\gamma}_\epsilon|^m \leq \mathcal{C}(\sqrt{3}N_B)^m, \tag{6.4}$$

since $|n_i|$ is strongly bound by the number of rows of Q, which in turn implies that the summation $\mathcal{C} = \sum_{\boldsymbol{n}} |c_{\boldsymbol{n}}|$ is finite. Rearranging Eq.(6.3) to express the lowest order homogeneous polynomial in the higher order polynomials we obtain the estimate

$$\begin{aligned} |P_3(\hat{\gamma}_\epsilon)| &\leq \frac{3!}{\epsilon^3}\mathcal{C}\sum_{m\geq 2}\frac{\epsilon^{2m+1}}{(2m+1)!}(\sqrt{3}N_B)^{2m+1} \\ |P_4(\hat{\gamma}_\epsilon)| &\leq \frac{4!}{\epsilon^4}\mathcal{C}\sum_{m\geq 3}\frac{\epsilon^{2m}}{(2m)!}(\sqrt{3}N_B)^{2m} \end{aligned}, \tag{6.5}$$

Version of February 24, 2017– Created February 24, 2017 - 19:08

taking $\epsilon = 0$ on both sides we obtain

$$P_3(\hat{\gamma}_0) = 0 \quad \text{and} \quad P_4(\hat{\gamma}_0) = 0, \tag{6.6}$$

where

$$\hat{\gamma}_0 = \lim_{\epsilon \to 0} \frac{\epsilon \hat{\gamma}_\epsilon}{\epsilon} = \lim_{\epsilon \to 0} \frac{\gamma(\epsilon) - \gamma(0)}{\epsilon} = \left. \frac{d\gamma}{d\epsilon} \right|_{\epsilon=0}. \tag{6.7}$$

□

The logical inversion of this lemma, together with the conjecture, gives us the following theorem:

Theorem 2. *If a system described by a rigidity matrix Q does not have any soft directions, then the system cannot have Weyl structures.*

Now what is left is a matter of letting the computer calculate the number of soft directions for different values of ψ, ϕ and θ. We have plotted the result of such sweeps in figures Fig.6.2 and Fig.6.3. In the first figure we see that a region of phase space around $\psi = \phi = \pi/3$ and $\theta = 0$ do not have any soft directions. In the second figure we have plotted the number of soft directions corresponding to configurations with *all* three angles non-zero. From this figure we observe that the zero-soft-direction region does not extend (deeply) into the $\theta \neq 0$ regime. Furthermore, our investigation in the $\psi, \phi, \theta \neq 0$ cube indicates

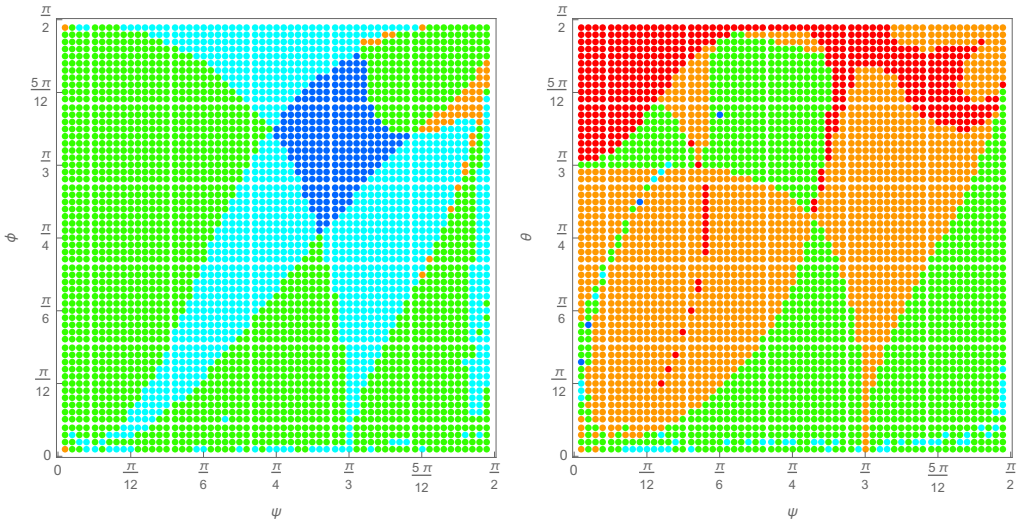

Figure 6.2: *Phase space plot showing the number of soft directions for different values of ψ and ϕ (left) or ψ and θ (right), where the third angle is kept at zero. The colors represent the existence of 0 (blue), 2 (cyan), 4 (green), 6 (orange) or $\geq$8 (red) soft directions at the origin of the Brillouin zone.*

Version of February 24, 2017– Created February 24, 2017 - 19:08

that soft-direction-less lattices are relatively rare, with our rough search returning the estimates for the soft-direction count distribution as expressed in Table 6.1.

This rareness makes it all the more exciting to find such a relatively large (though thin) region of parameter-space around $\psi, \phi = \pi/3$ and $\theta = 0$, where the energy spectra of the corresponding lattices are completely devoid of any soft-directions at the origin, and thus devoid of Weyl structures.

Number of soft directions:	0	2	4	6	8	10	12
Percentage of phase space:	<0.1	20.0	53.5	17.3	6.9	2.2	<0.1

Table 6.1: *Estimate for the distribution of the number of soft directions over the cube where all three angle-parameters are strictly positive.*

Figure 6.3: *Phase space plot of configurations where all three angles are strictly positive. The seven images form a partition of the cube each showing those points with the same number of soft directions at the origin, with the number of soft directions included underneath.*

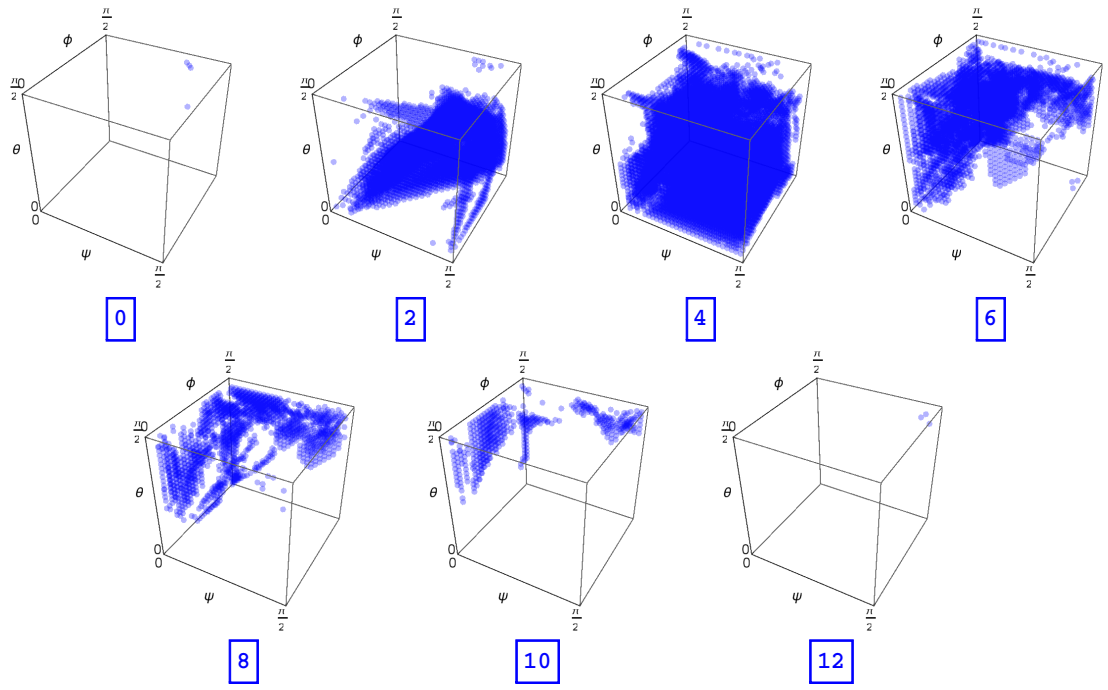

Version of February 24, 2017– Created February 24, 2017 - 19:08

6.2 Gapped lattice

We have found a region of space where the lattice is gapped throughout the Brillouin zone (apart from the origin). The lattice is quite deformed indeed, to a point where it becomes difficult to recognise the original triangular prism. We show the unit cell in Fig.6.4 and a section of the full lattice in Fig.6.5.

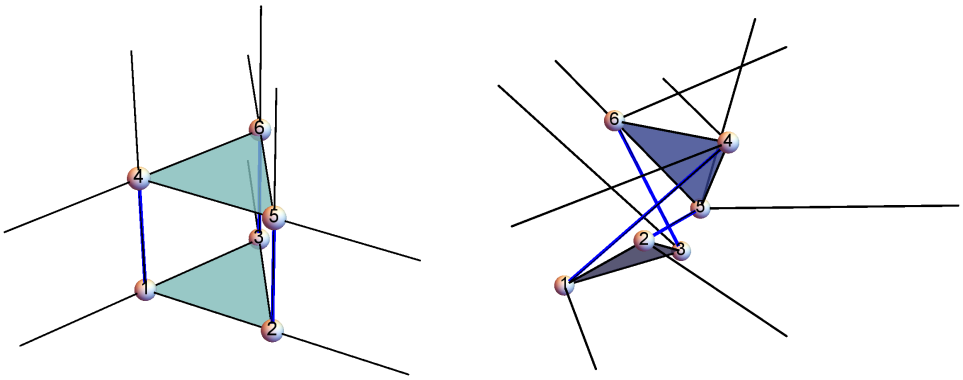

Figure 6.4: *Comparing the unit cell of the twisted kagome lattice (right) under the rotations $\psi = \phi = \pi/3$ versus to the canonical, unperturbed stacked kagome unit cell (left).*

Figure 6.5: *A section of $3 \times 3 \times 3$ unit cells of the twisted stacked kagome lattice.*

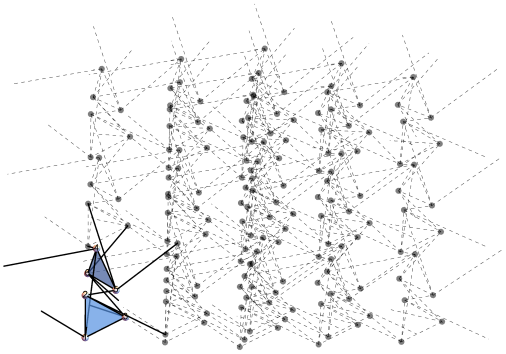

To our good fortune, we find that the lattice is non-trivially polarized. From the plots of the phase of the rigidity matrix in Fig.6.6 we can read that the winding numbers are $m_1 = m_2 = 0$ and $m_3 = 1$. Thus our polarization vector is

Version of February 24, 2017– Created February 24, 2017 - 19:08

given as

$$\boldsymbol{P} = \boldsymbol{a}_3. \tag{6.8}$$

Let us interpret this result in terms of zero-energy boundary modes. The expression for the determinant of the rigidity matrix at $\psi, \phi = \pi/3, \theta = 0$ takes the form of

$$\det Q_{\psi,\phi=\pi/3}(z_1, z_2, z_3) \propto \frac{\mathcal{Q}(z_1, z_2, z_3)}{z_1^2 z_2^2}, \tag{6.9}$$

where $\mathcal{Q}$ is a polynomial quartic in both z_1 and z_2 and cubic in z_3. First suppose we have an edge perpendicular to $\boldsymbol{a}_3$. We set $z_1 = e^{ik_1}$, $z_2 = e^{ik_2}$ where we interpret k_1 and k_2 as the wave numbers along the 2-dimensional edge. Since the determinant is polynomial in z_3 and thus has zero poles, we expect to see

$$n_3^{right} = m_3 + p_3^{right} = 1 \tag{6.10}$$

zero-energy edge mode on the side where $\boldsymbol{a}_3$ points outwards. By the fundamental theorem of algebra we know that the number of roots must equal the degree. As $\mathcal{Q}$ is cubic in z_3 we expect to find the remaining two zero energy edge modes on the opposite side. For z_1 and z_2 the determinant goes as $z_i^{-2}\mathcal{Q}(z_i)$, thus we have a second-order pole at the origin. Therefore we predict

$$n_i^{right} = m_i + p_i^{right} = 2 \qquad (i = 1, 2) \tag{6.11}$$

zero-energy edge modes on all vertically oriented sides. The claim of being completely gapped is now equivalent to saying that the number of zero-energy edge-modes is invariant under variations in the remaining two k_i. These predictions can be checked against the plots of the zero-energy edge mode bands contained in Fig.6.7.

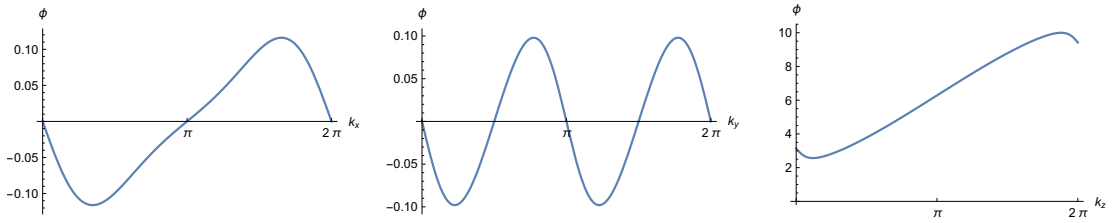

Figure 6.6: *The phase of the rigidity matrix along the directions k_1 (left), k_2 (middle) and k_3 (right) with the other two wave numbers fixed at π.*

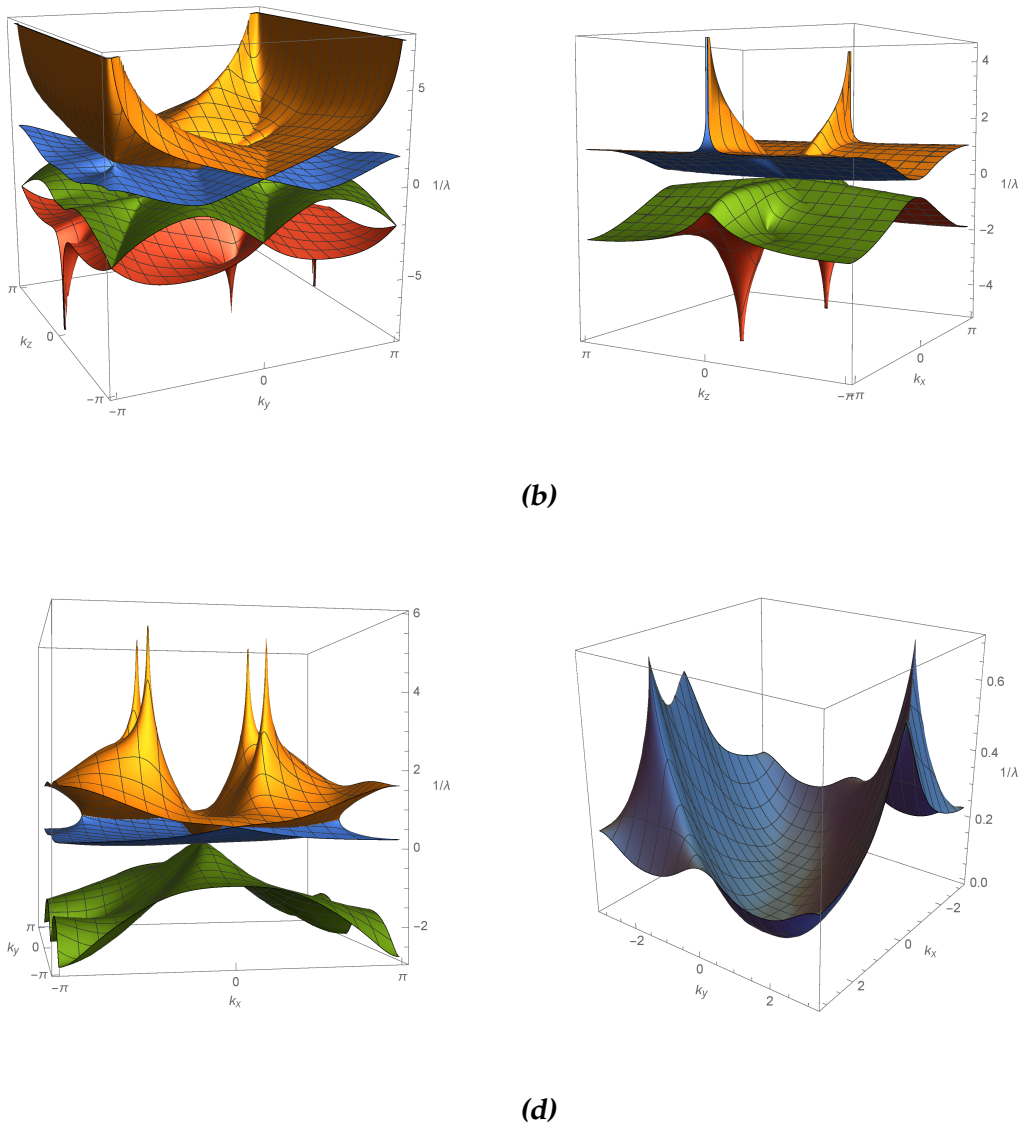

(a) ***(b)***

(c) ***(d)***

Figure 6.7: *Zero-energy edge modes plots for the gapped stacked kagome lattice at $\psi, \phi = \pi/3$. The vertical axis indicates the inverse penetration depth $1/\lambda = \ln|z_i|$ where negative (positive) λ indicates modes bound to the right (left) edge. Figures (a) through (c) show all zero-energy edge mode bands for edges perpendicular to respectively the $\hat{x}$, $\hat{y}$ or $\hat{z}$ axis. Note that the top two bands (yellow and blue) in figure (b) seem to coincide. Figure (d) shows the middle band for the $\hat{z}$-edge to illustrate its strictly increasing behaviour in the relevant regions.*

Version of February 24, 2017– Created February 24, 2017 - 19:08

Chapter 7

Dislocations in 3D lattices

7.1 Line dislocations

Now let us see how our lattice reacts to dislocations. We recall from section 3.4 that a dislocation is fully defined by a displacement function $\boldsymbol{u}(\boldsymbol{x})$. But if we choose the locus of singularities of the displacement function to be a line $L = \{\boldsymbol{\ell}(s) : s \in \mathbb{R}\}$, then the essential features of the dislocation are described by two geometrical quantities: the line direction $d\boldsymbol{\ell}$ and the Burgers vector $\boldsymbol{b}$.

We distinguish two principal cases. If the Burgers vector is orthogonal to the dislocation line, we have a stacking of the familiar two-dimensional dislocation. The Burgers vector pushes the unit cells apart in such a way that, to complete the lattice, we must add a half-plane of unit cells orthogonal to the Burgers vector and terminating in the dislocation line, see Fig.7.1a. This termination edge gives the dislocation the name edge dislocation.

On the other hand, if the Burgers vector is parallel to the dislocation line

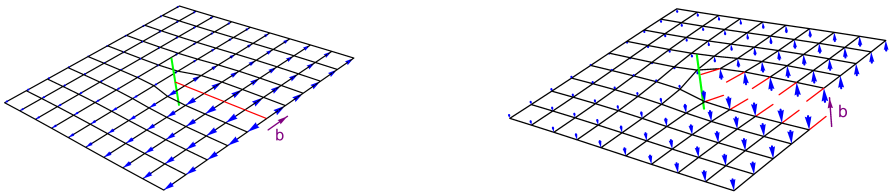

(a) *Edge dislocation* ***(b)*** *Screw dislocation*

Figure 7.1: *Example of the two principal types of line dislocations on a square lattice. Only one sheet of the three-dimensional lattice is depicted.*

no such adding of unit cells is needed. Simply reconnecting the side that was pushed upwards to the side that was pushed downwards one sheet higher will result in a smooth lattice, see Fig.7.1b. The resulting geometry resembles a screw and hence takes its name.

In regards to rigidity charges associated to these dislocation structure we can formulate the following theorem

Theorem 3. *The rigidity charge associated to line defects in a gapped, polarized Maxwellian lattice can be expressed in terms of the polarization vector of the undistorted lattice, the Burger's vector characterizing the type of line defect, and the direction of the line.*

Proof. We start from Eq.(3.32), that is

$$V_{cell} \cdot \nu_T^S = \int_{\partial S} d^2S\, \hat{n}_i \left(P_j \partial_j u_i - P_i \partial_j u_j\right). \tag{7.1}$$

Writing the surface elements explicitly in terms of the canonical coordinate basis we have

$$-d^2S\, \hat{n}_i := df_i = \tfrac{1}{2}\epsilon_{i\ell k} dx^\ell \wedge dx^k \quad \text{conversely} \quad dx^\ell \wedge dx^k = \epsilon^{i\ell k} df_i. \tag{7.2}$$

Some Levi-Civita tensor manipulations then allows us to rewrite Eq.(3.32) to

$$\begin{aligned} V_{cell} \cdot \nu_T^S &= \int_{\partial S} (-df_i) \left(P_j \partial_j u_i - P_i \partial_j u_j\right) = P_i \int_{\partial S} \left(\partial_i u_j df_j - \partial_j u_j df_i\right) \\ &= P_i \int_{\partial S} df_m\, 2\delta^m_{[i}\delta^\ell_{j]}\, \partial_\ell u_j = P_i \int_{\partial S} df_m\, \epsilon^{m\ell k}\epsilon_{ijk}\, \partial_\ell u_j \\ &= P_i \int_{\partial S} \epsilon_{ijk}\, \partial_\ell u_j\, dx^\ell \wedge dx^k = P_i \int_{\partial S} \epsilon_{ijk}\, du_j \wedge dx^k. \end{aligned} \tag{7.3}$$

Now we impose our particular geometry. Consider a straight line segment of the dislocation line and orient our basis such that it points in the $\hat{z}$ direction, that is $L = \mathbb{R}\hat{z}$. We can take S to be the cylinder with radius $\mathcal{R}$ centred at and aligned with L. If the cylinder respects the periodicity of our lattice the top and bottom surface integrals will cancel by orientation. The sides of the cylinder can then be decomposed in horizontal circles C_z at varying height z or in vertical lines L_θ at varying angle θ. With these decompositions we find:

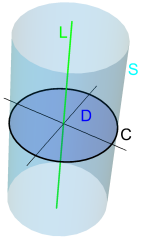

$$\begin{aligned} V_{cell} \cdot \nu_T^S &= P_i \int_{-s}^{s} \epsilon_{ij3}\, dz \int_{C_z} du_j + P_i \int_0^{2\pi} d\theta\, \epsilon_{ij2}\mathcal{R}\cos\theta - \epsilon_{ij1}\mathcal{R}\sin\theta \int_{L_\theta} du_j \\ &= P_i \epsilon_{ij3} \int_{-s}^{s} dz\, b_j + P_i \int_{L_0} du_j \int_0^{2\pi} d\theta\, \epsilon_{ij2}\mathcal{R}\cos\theta - \epsilon_{ij1}\mathcal{R}\sin\theta \\ &= \int d\hat{\boldsymbol{\ell}} \cdot (\boldsymbol{P} \times \boldsymbol{b}). \end{aligned} \tag{7.4}$$

Version of February 24, 2017– Created February 24, 2017 - 19:08

□

Keeping with our analogy with the electromagnetic case, we can treat the quantity $\boldsymbol{d} = \boldsymbol{b} \times \int d\hat{\boldsymbol{\ell}}$ as a rigidity dipole moment, giving us the relation

$$V_{cell} \cdot \nu_T^S = \boldsymbol{P} \cdot \boldsymbol{d} \tag{7.5}$$

Most importantly we see that screw dislocations have zero-dipole, as by definition their Burgers vector is parallel to the dislocation line. As such we come to understand that the screw dislocation does not carry any net rigidity charge. Since the proof of the theorem is locally valid, this seems to imply that no charges at all are associated to the screw dislocation.

For the edge dislocation we obtain a result that reduces to the result obtained in [1] when restricted to two dimensions.

7.2 Screw dislocation in polarized Kagome

To test our claims that screw dislocations are charge-free we numerically calculate the energy spectrum of a screwed stacked kagome lattice. When talking about screws we have to make the distinction between right-handed and left-handed screws, or screws and antiscrews.

In the first case, clockwise paths around the dislocation line will move you up, while for antiscrews anticlockwise paths move you up. Equivalently we can define screws as having their burgers vector align with the line direction, while in the antiscrew case the burgers vector points in the opposite direction.

The lovely thing about screws and antiscrews is that square cut-outs of these screws can be glued together smoothly as shown in Fig.7.2a. This allows us

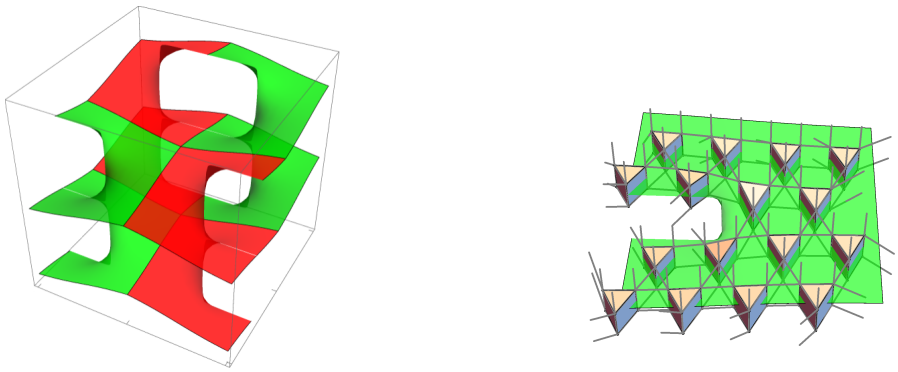

(a) *Screw-antiscrew displacement function.* ***(b)*** *SKL displaced under screw-dislocation.*

Figure 7.2: *The geometry of the screw-antiscrew displaced SKL unit cell.*

to consider a giant meta unit cell containing one level of two screws and two antiscrews in the checker-board pattern.

In Fig.7.2b we show a close-up of how the stacked kagome lattice would be deformed in the case that the dislocation line is vertical. One segment of a screw consists of $(2\mathrm{N})^2$ kagome unit cells around the dislocation line, such that a complete meta unit cell, containing four screws, consists of $4(2\mathrm{N})^2$ kagome unit cells. Explicit visualizations of these meta unit cells for both horizontal and vertical dislocation lines are given in Fig.7.3 for $\mathrm{N} = 3$.

Since each stacked kagome unit cell contains 6 sites the screw-antiscrew meta unit cell contains $6 \cdot 4(2\mathrm{N})^2$ sites, hence the dynamical matrix $D = Q^T Q$ has

$$N_B = dN = 3 \cdot 6 \cdot 4(2\mathrm{N})^2 = 288\mathrm{N}^2 \tag{7.6}$$

rows and columns. We consider the case $\mathrm{N} = 6$ in which we find 10.368 eigenvalues. Out of these eigenvalues at least three are zero, corresponding to the three rigid body translations. In Fig.7.4 it can be seen that these remain the only zero-modes in the screwed lattice.

Since zero-modes and states of self-stress can only be produced in pairs in accordance with Eq.(2.9), this means that the screw does not introduce any zero-modes or states of self-stress to the lattice.

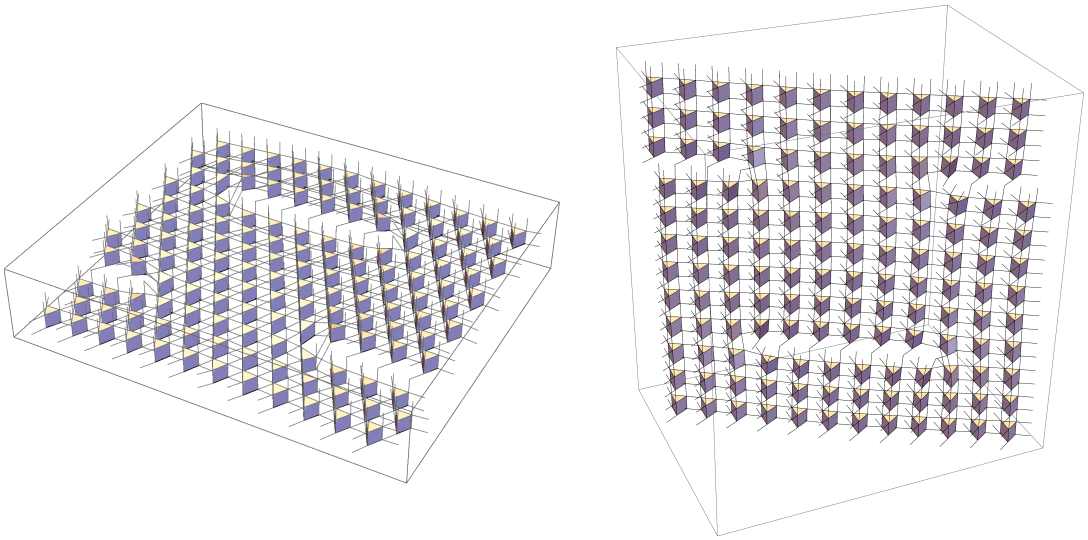

(a) *Vertical screw-antiscrew unit cell.* ***(b)*** *Horizontal screw-antiscrew unit cell.*

Figure 7.3: *Two types of screw-antiscrew meta unit cells with* $\mathrm{N} = 3$. *The vertical and horizontal refer to the direction of the dislocation line. Each prism represents a stacked kagome unit cell. For ease of reading the unit cells are drawn in the* $\psi, \phi, \theta = 0$ *configuration.*

Version of February 24, 2017– Created February 24, 2017 - 19:08

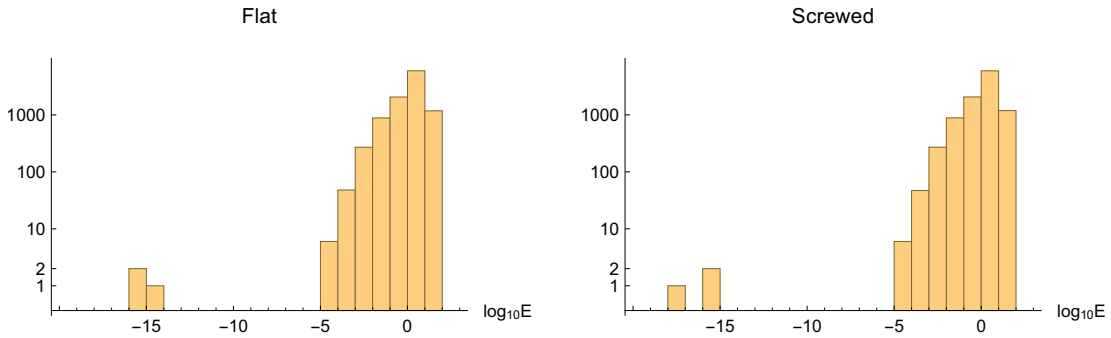

(a) *Horizontal screw-antiscrew meta unit cell compared to a similar flat meta unit cell.*

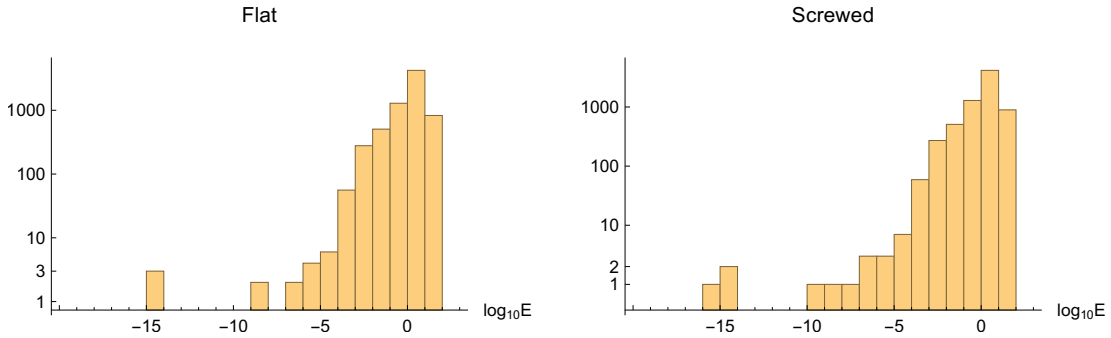

(b) *Vertical screw-antiscrew meta unit cell compared to a similar flat meta unit cell.*

Figure 7.4: *Histograms of the energy-eigenvalues corresponding to four meta unit cells, all with* $\mathrm{N} = 6$*. The vertical axis shows the occurrence of eigenvalues in the range given on the horizontal axis. All four graphs show a total of 3 eigenvalues around* 10^{-15}*, far removed from the rest of the spectrum.*

7.3 Dislocation loops

One final geometry we want to mention is that of the dislocation loops. Instead of an infinite dislocation line, we can think of bending the line into a closed path. It is important to realize that the Burgers vector would be constant around the path and that the polarization vector of the undisturbed lattice is constant throughout space. As such the topological charge of each line segment is given by the orientation of the line direction with respect to these quantities.

In particular, the gapped stacked kagome lattice has a polarization of $\boldsymbol{P} = \boldsymbol{a}_3$, as calculated in Eq.(6.8). Interesting geometries will be perpendicular to this vector and hence must be horizontal. Thus suppose we have the horizontal loop with Burgers vector as depicted in geometry in Fig.7.5.

We note that the left and right side of the loop are screw dislocations, whereas

the top and bottom side are composite line dislocations. Traversing the loop in the canonical direction we see that the bottom is aligned in the $\boldsymbol{a}_1$ direction, while the top is oppositely aligned. As such we find $\int d\hat{\boldsymbol{\ell}} = \pm N_{cell}\boldsymbol{a}_1$, with the plus sign for the bottom line and the minus sign for the top line. Here N_{cell} counts the number of unit cells along the line. The charge associated to these two line pieces can be calculated to be

$$\nu_T^S = \frac{1}{V_{cell}} \int d\hat{\boldsymbol{\ell}} \cdot (\boldsymbol{P} \times \boldsymbol{b}) = \pm N_{cell} \frac{\boldsymbol{a}_1 \cdot (\boldsymbol{a}_3 \times \boldsymbol{a}_2)}{V_{cell}} = \mp N_{cell}. \tag{7.7}$$

So we observe that the bottom line carries one net state of self-stress per unit cell, while the top line carries one net zero-mode per unit cell. As such we see that line dislocations can be used to separate rigidity charges into finite regions in the material.

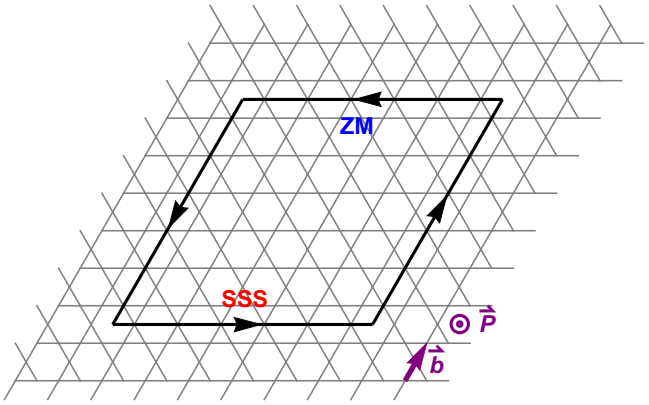

Figure 7.5: *The dislocation loop geometry projected on the kagome lattice.*

Version of February 24, 2017– Created February 24, 2017 - 19:08

Bibliography

[1] Jayson Paulose, Brian Ging-ge Chen, and Vincenzo Vitelli, *Topological modes bound to dislocations in mechanical metamaterials*, Nature Phys. **11**, 153 (2015).

[2] C. L. Kane and T. C. Lubensky, *Topological boundary modes in isostatic lattices*, Nature Phys. **10**, 39 (2014).

[3] Roman Süsstrunk and Sebastian D. Huber, *Classification of topological phonons in linear mechanical metamaterials*, Proc. Natl. Acad. Sci. **113**, 33 (2016)

[4] J. C. Y. Teo and C. L. Kane *Topological defects and gapless modes in insulators and superconductors* Phys. Rev. B **82**, 115120 (2010)

[5] Olaf Stenull, C. L. Kane, and T.C. Lubensky, *Topological phonons and Weyl lines in three dimensions*, Phys. Rev. Lett. **117**, 068001 (2016)

[6] T. C. Lubensky, C. L. Kane, Xiaoming Mao, A Souslov and Kai Sun, *Phonons and elasticity in critically coordinated lattices* Reports on Progress in Physics, **78**, 7 (2015)

[7] D. Zeb Rocklin, *Directional mechanical response in the bulk of topological metamaterials*, arXiv preprint arXiv:1612.00084v1 (2016)

[8] D. Zeb Rocklin, Shangnan Zhou, Kai Sun, and Xiaoming Mao, *Transformable topological mechanical metamaterials*, Nature Comm., **8**:14201 (2017)

[9] Joshua E. S. Socolar, Tom C. Lubensky and Charles L. Kane, *Mechanical Graphene*, arXiv prepring arXiv:1610.05787 (2016)

[10] L. D. Landau and E. M. Lifschitz, *Theory of Elasticity*, Pergamon Press Ltd., 2nd ed. (1970).

[11] J. C. Maxwell, *On the calculation of the equilibrium and stiffness of frames*, Philos. Mag., **27**:294, (1864)

[12] C. R. Calladine, *Buckminster Fuller "tensegrity" structures and Clerk Maxwell rules for the construction of stiff frames.*, Int. J. Solids Struct., **14(2)**:161-172, 1978

Appendix A

Appendix

A.1 Discrete functions are constant iff continuous

Theorem 4. *A function from a connected set to a discrete set is continuous if and only if it is constant, that is*

$$\underset{\textit{connected}}{X} \xrightarrow{g} \underset{\textit{discrete}}{Y} \quad : \quad g = \textit{continuous} \iff g = \textit{constant}. \tag{A.1}$$

Proof. Let g be a continuous function from the connected topological space $(X, \mathcal{T}_X)$ to the discrete topological space $(Y, \mathcal{T}_Y)$. The topological definitions of discreteness and continuity are respectively

$$\forall y \in Y : \{y\} \in \mathcal{T}_Y \quad \text{and} \quad \forall U \in \mathcal{T}_Y : g^{-1}(U) \in \mathcal{T}_X, \tag{A.2}$$

where $g^{-1}(U)$ denotes the pre-image of U under g. Suppose w.l.o.g. that X is non-empty, take any element $x^* \in X$ and compute $y^* = g(x^*)$. Then by continuity and discreteness the following sets are open in X (i.e. elements of $\mathcal{T}_X$):

$$U = g^{-1}(\{y^*\}) \quad \text{and} \quad V = \bigcup_{y \in Y \setminus \{y^*\}} g^{-1}(\{y\}). \tag{A.3}$$

By the single-valuedness of g it is immediate that $U \cap V = \emptyset$, further we note that $U \cup V = g^{-1}(Y) = X$. Thus, by the topological definition of connectedness

$$\forall U, V \in \mathcal{T}_X \setminus \{\emptyset\} : \quad U \cup V = X \quad \Rightarrow \quad U \cap V \neq \emptyset \tag{A.4}$$

and the fact that $X \neq \emptyset$ we conclude that $V = \emptyset$. That is, if $y \neq y^*$ there is no $x \in X$ such that $g(x) = y$, or in other words $\forall x \in X : g(x) = y^*$. Thus g is constant.

Conversely let $g : X \to Y$ be constant, that is

$$\exists y^* \in Y : \forall x \in X : g(x) = y^*, \tag{A.5}$$

then continuity is easily checked by

$$\forall U \in \mathcal{T}_Y : g^{-1}(U) = \begin{cases} X & \text{if } y^* \in U \\ \emptyset & \text{if } y^* \notin U \end{cases} \tag{A.6}$$

and the fact that $\emptyset, X \in \mathcal{T}_X$ by the definition of topology. □

A.2 Generalized stacked kagome: explicit formulas

In this section we list some explicit forms pertaining to the definition of the generalized stacked kagome lattice. First, the primitive vectors are unchanged from Eq.(4.1). Second, the equilibrium positions of the sites are explicitly

$$\begin{aligned}
\boldsymbol{R}(1^+,4^-) &= \frac{a}{2\sqrt{3}} \begin{pmatrix} \pm s_\psi c_\theta - \sqrt{3} c_\psi c_\phi - c_\psi s_\phi s_\theta \\ -c_\psi c_\theta \mp \sqrt{3} s_\psi c_\phi \mp s_\psi s_\phi s_\theta \\ \mp c_\phi s_\theta \pm \sqrt{3} s_\phi \pm \sqrt{3} \end{pmatrix} \pm \frac{ar}{2} \begin{pmatrix} c_\alpha \\ s_\alpha \\ 0 \end{pmatrix} \\
\boldsymbol{R}(2^+,5^-) &= \frac{a}{2\sqrt{3}} \begin{pmatrix} \pm s_\psi c_\theta + \sqrt{3} c_\psi c_\phi - c_\psi s_\phi s_\theta \\ -c_\psi c_\theta \pm \sqrt{3} s_\psi c_\phi \mp s_\phi s_\phi s_\theta \\ \mp c_\phi s_\theta \mp \sqrt{3} s_\phi \pm \sqrt{3} \end{pmatrix} \pm \frac{ar}{2} \begin{pmatrix} c_\alpha \\ s_\alpha \\ 0 \end{pmatrix} \\
\boldsymbol{R}(3^+,6^-) &= \frac{a}{\sqrt{3}} \begin{pmatrix} \mp s_\psi c_\theta + c_\psi s_\phi s_\theta \\ c_\psi c_\theta \pm s_\psi s_\phi s_\theta \\ \pm c_\phi s_\theta \pm \sqrt{3}/2 \end{pmatrix} \pm \frac{ar}{2} \begin{pmatrix} c_\alpha \\ s_\alpha \\ 0 \end{pmatrix}
\end{aligned} \tag{A.7}$$

where $s. = \sin(\cdot)$, $c. = \cos(\cdot)$ allows for a compact notation. The eighteen bonds are then given in the form $[s_\beta, s'_\beta, \Delta\boldsymbol{\ell}_\beta]$ and can be divided into six groups as follows:

Bottom horizontal internal:	$[2,3,(0,0,0)]$	$[3,1,(0,0,0)]$	$[1,2,(0,0,0)]$
Bottom horizontal external:	$[3,2,(-1,1,0)]$	$[1,3,(0,-1,0)]$	$[2,1,(1,0,0)]$
Top horizontal internal:	$[5,6,(0,0,0)]$	$[6,4,(0,0,0)]$	$[4,5,(0,0,0)]$
Top horizontal external:	$[6,5,(-1,1,0)]$	$[4,6,(0,-1,0)]$	$[5,4,(1,0,0)]$
Vertical internal:	$[1,4,(0,0,0)]$	$[2,5,(0,0,0)]$	$[3,6,(0,0,0)]$
Vertical external:	$[4,1,(0,0,1)]$	$[5,2,(0,0,1)]$	$[6,3,(0,0,1)]$

Version of February 24, 2017– Created February 24, 2017 - 19:08

Internal bonds connect sites within the same unit cell, whereas external bonds connect sites in different unit cells, as can be read from the third term in their bond description.

Following the order of enumeration from the above bond table, the compatibility matrix takes the form

$$C(\boldsymbol{q}) = \left(\begin{array}{c|ccc|ccc} \hat{\boldsymbol{b}}_1^T & 0 & -1 & 1 & & & \\ \hat{\boldsymbol{b}}_2^T & 1 & 0 & -1 & & O & \\ \hat{\boldsymbol{b}}_3^T & -1 & 1 & 0 & & & \\ \hline \hat{\boldsymbol{b}}_4^T & 0 & e^{-\imath \boldsymbol{q}\cdot\boldsymbol{a}_1} & -1 & & & \\ \hat{\boldsymbol{b}}_5^T & -1 & 0 & e^{-\imath \boldsymbol{q}\cdot\boldsymbol{a}_2} & & O & \\ \hat{\boldsymbol{b}}_6^T & e^{-\imath \boldsymbol{q}\cdot\boldsymbol{a}_{12}} & -1 & 0 & & & \\ \hline \hat{\boldsymbol{b}}_7^T & & & & 0 & -1 & 1 \\ \hat{\boldsymbol{b}}_8^T & & O & & 1 & 0 & -1 \\ \hat{\boldsymbol{b}}_9^T & & & & -1 & 1 & 0 \\ \hline \hat{\boldsymbol{b}}_{10}^T & & & & 0 & e^{-\imath \boldsymbol{q}\cdot\boldsymbol{a}_1} & -1 \\ \hat{\boldsymbol{b}}_{11}^T & & O & & -1 & 0 & e^{-\imath \boldsymbol{q}\cdot\boldsymbol{a}_2} \\ \hat{\boldsymbol{b}}_{12}^T & & & & e^{-\imath \boldsymbol{q}\cdot\boldsymbol{a}_{12}} & -1 & 0 \\ \hline \hat{\boldsymbol{b}}_{13}^T & & & & & & \\ \hat{\boldsymbol{b}}_{14}^T & & -I & & & I & \\ \hat{\boldsymbol{b}}_{15}^T & & & & & & \\ \hline \hat{\boldsymbol{b}}_{16}^T & & & & & & \\ \hat{\boldsymbol{b}}_{17}^T & & e^{-\imath \boldsymbol{q}\cdot\boldsymbol{a}_3} I & & & -I & \\ \hat{\boldsymbol{b}}_{18}^T & & & & & & \end{array}\right) \tag{A.8}$$

where $\boldsymbol{a}_{12} = \boldsymbol{a}_2 - \boldsymbol{a}_1$. The notation should be interpreted that each number in the matrix grid multiplies the triple on the far left in the same row. Check that this turns the matrix into a 18 by 18 square matrix. The bond directions $\hat{\boldsymbol{b}}_\beta$ are defined in terms of the equilibrium positions $\boldsymbol{R}(s)$ in Eq.(2.20).

Version of February 24, 2017– Created February 24, 2017 - 19:08

A.3 One-parameter deformation calculations

The determinant for the rigidity matrix for a tilt under the angle θ is

$$\det Q_\theta(z_1,z_2,z_3) = -\frac{1}{2^6}(z_1z_2)^{-2}(1-z_1)^2(1-z_3)^3(2-\cos\theta)^2(2+\cos^2\theta)^2\cos^2\theta \cdot(4\cos^2\theta-1)[z_1(z_2-\cos\theta)+z_2(1-2z_2+z_2\cos\theta)]^2, \tag{A.9}$$

where we readily observe the $k_1 = 0$ and $k_3 = 0$ planes. The term in square brackets involving z_2 involves a sum of two complex numbers. This can only be zero if the modulus of both numbers are equal, which gives the requirement

$$0 = |z_2-\cos\theta|^2 - |1-2z_2+z_2\cos\theta|^2 = -4(1-\cos\theta)(1-\Re z_2), \tag{A.10}$$

where we used $|z_i| = 1$. For non-zero θ this restricts z_2 to 1, which after substitution into the bracketed expression gives $(z_1-1)(\cos\theta-1) = 0$. Hence, this term is zero only on the line $k_1 = k_2 = 0$, which is already included in the $k_1 = 0$ plane. Further note that Eq.(A.9) is identically zero on the entire Brillouin zone when $\cos\theta = \frac{1}{2}$ or $\cos\theta = 0$. The former is because the rotation under $\theta = \pi/3$ maps the sites $s = 3$ and $s = 6$ on top of each other, effectively causing a bond to disappear from the unit cell. In the latter case the planes have tilted 90° towards each other and now form a 2D-structure.

Next, for non-zero ϕ we find

$$\det Q_\phi(z_1,z_2,z_3) = -\frac{3^3}{2^6}(z_1z_2)^{-2}(1-z_1)^2(1-z_3)^3(2-\cos\phi)^2\cos^6\phi \cdot[z_1(\cos\phi-2+z_2)+z_2(1-z_2\cos\phi)]^2. \tag{A.11}$$

Again we have the planes $k_1 = 0$ and $k_3 = 0$. By the same argument as above, the bracketed term does not contribute any new zero-mode structures, and $\phi = \pi/2$ causes the two triangles to be coplanar.

Finally for non-zero ψ we have

$$\det Q_\psi(z_1,z_2,z_3) = -\frac{3^2}{2^6}(z_1z_2)^{-2}(1-z_3)^3(5-4\cos\psi)^2 \cdot\Big[3(1-z_1)^2(1-z_2)^2(z_1-z_2)^2(1-2\cos\psi)^2 - 4[(z_1^2+z_2)(1+z_2)+z_1(1-6z_2+z_2^2)]^2\sin^2\psi\Big]. \tag{A.12}$$

Let us first treat the case where $\psi = \pi/3$. For this value the determinant simplifies to

$$\det Q_{\psi=\frac{\pi}{3}}(z_1,z_2,z_3) = \frac{3^4}{2^6}\frac{(1-z_3)^3}{(z_1z_2)^2}[(z_1^2+z_2)(1+z_2)+z_1(1-6z_2+z_2^2)]^2, \tag{A.13}$$

Version of February 24, 2017– Created February 24, 2017 - 19:08

which vanishes on the $k_3 = 0$ plane and wherever the expression in the square brackets equals zero. For the bracketed term we note the inequality

$$|z_1^2 + z_2| \cdot |1 + z_2| \leq 4 \leq |1 - 6z_2 + z_2^2|, \tag{A.14}$$

with equality if and only if $z_1 = z_2 = 1$. A quick substitution in Eq.(A.12) shows that the line $k_1 = k_2 = 0$ is indeed a line of zeroes of the determinant. In fact, together with the $k_3 = 0$ plane it is the only location where the determinant vanishes for any $\psi \neq 0$.

To show that $\psi \neq \pi/3$ does not have any other zero-points, we note that these points would satisfy

$$\frac{2}{\sqrt{3}} \frac{\sin\psi}{1 - 2\cos\psi} = \pm \frac{(1 - z_1)(1 - z_2)(z_1 - z_2)^2(1 - 2\cos\psi)}{(z_1^2 + z_2)(1 + z_2) + z_1(1 - 6z_2 + z_2^2)}. \tag{A.15}$$

Note that the cases we treated above are exactly the cases for which one of the divisions on either side becomes ill-defined. Now all is left is the observation that the left-hand side is obviously real and non-zero, whereas the left hand side is completely imaginary. This can be seen by using $\alpha/\beta \in \imath\mathbb{R} \iff \alpha^*\beta \in \imath\mathbb{R}$ and a direct but tedious calculation giving

$$\begin{aligned}(1 - z_1^*)(1 - z_2^*)(z_1^* - z_2^*)[(z_1^2 + z_2)(1 + z_2) + z_1(1 - 6z_2 + z_2^2)] \\ = 2\imath\,\Im\Big[z_2\left(|z_1^2 + z_2| + 2\Re(z_1) + 2\Re(z_1 z_2^*)\right)(1 - z_1^*)(7 - 7z_2 + z_2^2 - z_2^*)\Big].\end{aligned} \tag{A.16}$$

Thus Eq.(A.15) has no solutions for non-zero ψ.

Version of February 24, 2017– Created February 24, 2017 - 19:08

A.4 Relation between nullity and lowest order

In Chapter 6 we used the fact that the nullity of $Q(\mathbf{0})$ is at least $d = 3$ to argue that the expansion of $Q(\boldsymbol{k})$ around $\boldsymbol{k} = \mathbf{0}$ contains no constant, linear or quadratic term. This follows from the following general lemma.

Lemma 2. *Consider a smooth, matrix-valued function $A : \mathbb{R}^n \to \mathrm{Mat}_{m\times m}(\mathbb{C})$ and a point p in the domain of A, then*

$$|\alpha| < \mathrm{null}A(p) \quad \Rightarrow \quad (\partial^\alpha \det A)(p) = 0, \tag{A.17}$$

where $\alpha = (\alpha_1, \ldots, \alpha_n)$ is a multi-index, $|\alpha| := \sum_i \alpha_i$ and $\partial^\alpha := \partial_1^{\alpha_1} \cdots \partial_n^{\alpha_n}$.

Proof. For notational simplicity set $k = \mathrm{null}A(p)$. Every complex square matrix admits a singular value decomposition. That is

$$A(p) = USV^*, \tag{A.18}$$

where U, V are unitary matrices and S is the diagonal matrix with the singular values of $A(p)$ along the diagonal in ascending order. Since all vectors in the kernel of $A(p)$ are zero-eigenvectors of $A(p)^*A(p)$, we find that the first k entries on the diagonal of S are zero.

Using the unitary matrices U and V we can extend the singular matrix S to the matrix-valued function

$$S(x) = \big(\boldsymbol{s}_1(x), \ldots, \boldsymbol{s}_n(x)\big) := U^*A(x)V, \tag{A.19}$$

where the first k column vectors satisfy $\boldsymbol{s}_i(p) = \mathbf{0}$. Writing the determinant as a wedge product we can use the product rule to evaluate

$$\partial_i\big(\boldsymbol{s}_1(x) \wedge \cdots \wedge \boldsymbol{s}_m(x)\big) = \sum_j \boldsymbol{s}_1(x) \wedge \cdots \wedge \partial_i \boldsymbol{s}_j(x) \wedge \cdots \wedge \boldsymbol{s}_m(x). \tag{A.20}$$

For the higher-order derivative ∂^α we obtain a summation over $m^{|\alpha|}$ terms, where each term contains at most $|\alpha|$ differentiated column vectors. Since we assumed $|\alpha| < k$, this process leaves at least $k - |\alpha| \geq 1$ of the first k column vectors undifferentiated. Taking x to p, these undifferentiated column vectors evaluate to $\mathbf{0}$. Hence we find

$$\left(\partial^\alpha \det A\right)(p) = \det(UV^*) \cdot \left(\partial^\alpha \det S\right)(p) = 0. \tag{A.21}$$

□

Version of February 24, 2017– Created February 24, 2017 - 19:08